

Evolution of Neoproterozoic–Paleoproterozoic basement in the Brunovistulia terrane, S Poland: geological, *P-T* and geochemical records

Andrzej ŻELAŻNIEWICZ¹, * and Mirosław JASTRZĘBSKI¹

¹ Polish Academy of Sciences, Institute of Geological Sciences (ING PAS), Podwale 75, 50-449 Wrocław, Poland



Żelaźniewicz, A., Jastrzębski, M., 2021. Evolution of Neoproterozoic–Paleoproterozoic basement in the Brunovistulia terrane, S Poland: geological, *P-T* and geochemical records. *Geological Quarterly*, 65: 20, doi: 10.7306/gq.1590

Brunovistulia is a composite terrane of Gondwana descent that eventually was accreted to the SW margin of Baltica, central Europe. It is built of metagneous and metasedimentary rocks that originated mainly between 650 and 550 Ma. However in the Upper Silesian part of Brunovistulia, much older fragments have been drilled, which yielded U-Pb zircon ages between 2.75 and 2.0 Ga. They have been interpreted as an “exotic” constituent of the Brunovistulia superterrane, named the Rzeszotary Terrane. Our geological and geochemical studies of the Rzeszotary borehole cores yielded new data on the composition, provenance and evolution of that terrane. Precursors of the Rzeszotary complex were separated from the depleted mantle prior to or around 3.2–3.0 Ga. At 2.75–2.6 Ga, a juvenile magmatic arc edifice formed, beneath which oceanic lithosphere was subducted. Decompression melting of the mantle brought about tholeiite magmas of IAT/MORB composition with LILE additions. Tonalitic and trondhjemitic precursors of gneisses present today were formed at that time, probably due to partial melting of mantle-derived wet basalts at the base of the island arc. Around 2.0 Ga, the arc collided with an unspecified cratonic mass and was subject to orogenic deformation, metamorphism and migmatization. The entire arc edifice was then strongly shortened and forced down to depths equivalent to ~6–12 kbar where the rocks underwent contractional deformation and metamorphism (~500–700°C). Tonalites and trondhjemites were changed to gneisses, and basites to epidote- and garnet amphibolites. These rocks underwent syntectonic migmatization through the mechanism of segregation/differentiation in the presence of fluids and incipient partial melting. Synmetamorphic shortening of the rock pile, which led to folding and heterogeneous development of shear zones with thrust kinematics, terminated with intrusions of K-granites at 2.0 Ga, being followed by some brittle-ductile deformation of unconstrained timing. The 2.0 Ga event may have been connected with the 2.1–1.8 Ga global amalgamation of the Paleoproterozoic supercontinent of Columbia. Later the future Rzeszotary Terrane was detached from the Gondwana mainland, reassembled and eventually, in the Neoproterozoic, it became part of the foreland of the Cadomian Orogen in Central Europe.

Key words: back-arc, Brunovistulia, mantle, migmatite, Rzeszotary, Upper Silesia.

INTRODUCTION

Brunovistulia (Dudek, 1980; Finger et al., 2000; Kalvoda et al., 2003, 2008; Żelaźniewicz et al., 2009, 2020; Jastrzębski et al., 2021) is a composite terrane of Gondwana affinity that eventually was accreted to the SW margin of Baltica, Central Europe (Fig. 1). It is only partly exposed in the eastern Czech Republic and southern Poland. Similarities to units farther SE, in Moesia (Romania) and in the Istanbul-Zonguldak area (Turkey), allow speculation that these may link beneath the Carpathian nappes, a model verifiable only by subsurface geological and geophysical investigations (Haydutov and Yanev, 1995), or at least form a Brunovistulian group of terranes (Kalvoda and Bábek, 2010). In NW Brunovistulia, most of the parts already studied are built of metagneous and metasedimentary rocks that originated between 650 and 550 Ma (Finger

et al., 1995, 2000; Friedl et al., 2000; Oberc-Dziedzic et al., 2003; Żelaźniewicz et al., 2005, 2009; Jastrzębski et al., 2021). However in the Upper Silesian part of Brunovistulia (Fig. 1A), much older components have also been found, whose rocks yielded U-Pb zircon ages between 2.75 and 2.0 Ga (Żelaźniewicz and Fanning, 2020). Accordingly its tectonothermal evolution may be traced back to the Paleoproterozoic, which makes a striking contrast with the rest of Brunovistulia. On account of this and in view of the lack of younger ductile reworking, the oldest fragment was interpreted as one more ‘exotic’ constituent of the Brunovistulia superterrane (Fig. 1) and referred to as the Rzeszotary Terrane (Żelaźniewicz et al., 2009, 2020; Jastrzębski et al., 2021). This study focuses on rocks of the Rzeszotary Terrane and is aimed at shedding more light on their composition, provenance and evolution.

GEOLOGICAL FRAMEWORK

In the northeastern part of Brunovistulia (= the Upper Silesia Block, Fig. 1B), SW of the Kraków–Lubliniec Fault Zone (= border between Brunovistulia and Małopolska), crystalline rocks were encountered subsurface in a basement elevation

* Corresponding author, e-mail: pansudet@pwr.wroc.pl

Received: November 17, 2020; accepted: February 16, 2021; first published online: May 5, 2021

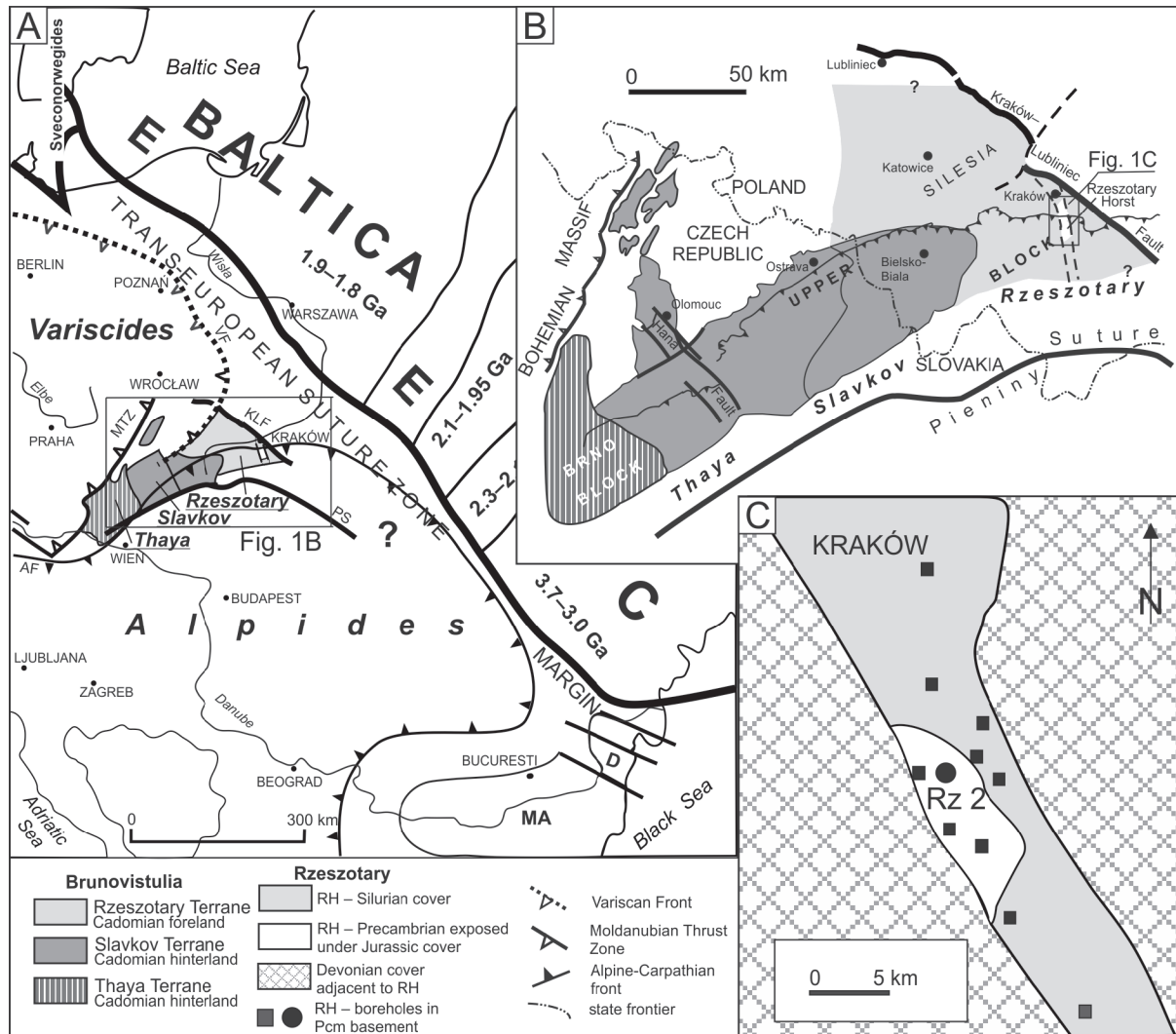


Fig. 1A – location of Brunovistulia (box) within a tectonic sketch of Central Europe; **B** – terranes in Brunovistulia; **C** – the Rzeszotary Horst (light grey) with the top part (white) exposed at the Jurassic palaeosurface, flanked by Devonian carbonates (grid)

Rz 2 borehole (dot), other boreholes (squares), modified after Konior (1974) and Żelaźniewicz and Fanning (2020); AF – Alpine Front, EEC – East European Craton, D – Dobrogea, KLF – Kraków–Lubliniec Fault Zone, MA – Moesia, MTZ – Moldanubian Thrust Zone, PS – Pieniny Klippen Belt, VF – Variscan Front

referred to as the Rzeszotary Horst (Konior, 1974; Heflik and Konior, 1974; Buła, 2000; Żelaźniewicz et al., 2009). The basement was first discovered in borehole Rzeszotary 1, south of Kraków (Fig. 1C). At its bottom (830–837 m), greenschists and muscovite orthogneisses were recorded. Neither the position and origin, nor significance, of those rocks was clear as they might have represented a solid basement or, alternatively, tectonic xenoliths incorporated within Carpathian thrust sheets during the formation of Miocene nappes (Petrascheck, 2009; Nowak, 1927). The rocks were found directly beneath 30 m of conglomerates and calcareous sandstones, with clasts of quartz and mica schist, that pass upwards into white limestones with remains of Jurassic echinoderms (Petrascheck, 2009). In 1960–61, borehole Rzeszotary 2 (Rz 2) was drilled 200 m east of the old one. In Rz 2, nearly 120 m of the crystalline basement (top at ~845 m b.t.l.) was penetrated below the Middle Jurassic–Cretaceous platform cover which in turn is overlain by Miocene deposits of the West Carpathian foredeep and topped tectonically by West Carpathian nappes

of the Alpine system (Burtan, 1962). In the Rzeszotary Horst, crystalline rocks, mainly felsic gneisses and granites, were also drilled in several other boreholes nearby (Fig. 1C). Lower Cambrian shallow marine clastic rocks were found to the west, and Devonian limestones to the east, of the horst (Konior, 1974; Buła, 2000). The horst may have developed around the Ediacaran–Cambrian transition as indicated by the presence of adjacent highly mature Lower Cambrian sandstones, and remained exposed until the Silurian. Alternatively, the horst emerged in the Devonian and stayed temporarily concealed. In few other boreholes in the area, the top of the basement rocks was reached at a depth of ~2100 m, which points to extensive block tectonics within the horst itself (Fig. 1C).

Felsic gneisses, ubiquitously drilled in the Rzeszotary Horst, form at least the upper layer of the Precambrian bedrock directly beneath the Phanerozoic sedimentary cover (Fig. 1C). Amphibolites were found only in one (Rz 2) of those boreholes (Konior, 1974). However the presence of mafic bodies deeper in the crust is probable. Potential field data support such a pos-

sibility, albeit ambiguously. On gravimetric maps (Królikowski and Petecki, 1995), a local, ~N–S elongate high (3–4 mgal) perfectly overlaps with the inferred Rzeszotary horst area. In contrast, on magnetic maps (Cieśla et al., 1993), this area coincides with a distinct low (~–50 nT), whereas a magnetic high (~100 nT) occurs west of this low and of the horst. However, Devonian diabases also occur in the area, and so the high may have been produced by them and not by the Precambrian metabasites. In view of that, we presume that the Precambrian crust is dominated by felsic rocks which alternate vertically/laterally with subordinate mafic rocks. It seems that in Rz 2, the amphibolite body is shallow enough to be detected in the gravimetric pattern but not voluminous enough to be matched by the magnetic pattern; thus the body is probably relatively thin, being set in dominantly felsic surroundings.

Zircons from the felsic gneisses have yielded U–Pb SHRIMP ages around 2.75–2.6 Ga (cores and single grains) and ~2.0 Ga (rims and single grains). The older ages are interpreted as the time of origin of the gneiss precursor, whereas the younger ages indicate metamorphism and migmatization. Late-orogenic unfoliated K-granite was emplaced in an extensional regime, which terminated the 2.0 Ga event. More details can be found in an earlier companion paper (Żelaźniewicz and Fanning, 2020).

METHODS

Rock samples were collected from borehole cores (9 cm). Samples crushed for zircons were also analysed geochemically. Their weight varied between 3.5 kg (felsic rocks) and 6 kg (mafic rocks). Before crushing, thin sections were prepared for microscopic and EPMA analyses and supplemented by those cut from additional small samples (30) that represented the main rock types.

Whole-rock major element and trace element analyses were carried out in Activation Laboratories, Ltd. in Ancaster, Ontario, Canada, via ICP–OES and ICP–MS techniques following lithium metaborate–tetraborate fusion of each sample at their facility. Sm–Nd isotopic compositions and abundances were measured in the same lab in static mode by *Multi-Collector ICP–Mass Spectrometry*. Compositions of constituent minerals were determined by EPMA in the lab of Warsaw University using a *CAMECA SX–100* with 15KV voltage and 12 nA current. Representatives of each of these rock types were analysed (Appendix 1*). *GCDkit 3.0* software (Janoušek et al., 2006) was used for drawing most of the geochemical diagrams, calculations of accessory mineral saturation temperatures for felsic rocks, and for calculations of Sm–Nd isotopic parameters.

P–T conditions of the formation of mineral assemblages in the amphibolites were estimated utilizing classic geothermobarometric methods developed by Hammarstrom and Zen (1986), Schmidt (1992), Holland and Blundy (1994) and Ravna (2000) and assessed by thermodynamic modeling with use of *THERMOCALC 3.33* (Holland and Powell, 1998, dataset 55). For the thermodynamic modeling of the amphibolite samples, $\text{Na}_2\text{O–CaO–FeO–MgO–Al}_2\text{O}_3\text{–SiO}_2\text{–H}_2\text{O–TiO}_2\text{–Fe}_2\text{O}_3$ (NCFMASHTO) system was used. This was considered to well reflect the chemical system of the amphibolites studied because of negligibly small quantities of K_2O (<0.63 wt.%) and MnO

(<0.21 wt.%) and lack of K-feldspar, K-bearing micas and Mn-rich garnets in the mineral composition (Appendix 1). Activity–composition models for the NCFMASHTO system followed those recommended on the THERMOCALC documentation page (available in 2019). Microprobe results and the A–X models used for analyses are listed in Appendix 2. The amount of ferric iron within the bulk composition was estimated at 5% of total Fe in both samples. Fe_2O_3 values were thus estimated at 0.46 wt.% in sample A1 and 0.74 wt.% in sample A2. Phase diagrams were calculated with H_2O in excess.

CHARACTERISTICS OF CRYSTALLINE ROCKS IN THE RZESZOTARY 2 BOREHOLE

In Rz 2, crystalline rocks were drilled at a depth interval of 847.5–965.1 m¹ (Fig. 2). An original description of the borehole log was published by Burtan (1962). Directly beneath the Jurassic cover, chlorite–muscovite schists with feldspar lenses (845.7–882.1 m) were reported which graded downwards to coarse-grained muscovite schists with feldspar veinlets and then to two-mica feldspar gneisses (882.1–886.3m). Deeper in the log profile, amphibolites with “feldspathic injections”, amphibole gneisses with mica schist intercalations and coarse-grained garnet amphibolite were observed (886–952 m). In the deepest interval (952–965.1 m), muscovite schists with abundant pink feldspathic injections and arterites (*sensu* Sederholm – Mehnert, 1968) were described, the schists being affected by tectonic movements. The rocks drilled were interpreted as a pre-Hercynian series of “more or less diaphoretically altered amphibolites and gneisses injected with feldspars and subjected to granitization, likely forming a mantle to a more deeply seated granite body” (Burtan, 1962).

Recent re-inspection of the Rzeszotary 2 borehole cores has shown that the above generalization requires some revision. In the ~120 m long section, poorly to strongly foliated, partly migmatized amphibolites and a variety of felsic gneisses and granites occur. Their relationships are shown in the reconstructed log profile (Fig. 2). The crystalline rocks are overlain unconformably by a ~10 m thick layer of grey, coarse to medium-grained calcarenite (Jurassic?) which contains some clasts of weathered mafic and felsic rocks, and then by zonally brecciated crinoidal limestones of mid-Jurassic age.

MAFIC ROCKS

The amphibolites are poorly to locally strongly foliated rocks (Fig. 3). In mineral composition, amphibole prevails over plagioclase whereas epidote, titanite, garnet and calcite occur as accessories, though in widely varying proportions.

Volumetrically dominant amphibolite type 1 (A1) is a massive coarse to medium-grained garnet-poor rock, probably derived from a gabbroic protolith (Figs. 2 and 3A, B). It consists of slightly compositionally zoned minerals: Ca-amphibole ($\text{Mg}\# = 0.66_{\text{core}} \ 0.61_{\text{rim}}$; $\text{Si}^{+4} = 6.71_{\text{c}} \ 6.48_{\text{r}}$, a.p.f.u.), plagioclase ($\text{An}_{22\text{c}} \ 5_{\text{r}}$), epidote ($\text{Ps}_{5.7\text{c}} \ 3.7_{\text{r}}$), titanite, \pm accessory garnet ($\text{Alm}_{58} \ 56\text{–} \text{Gr}_{29} \ 27\text{–} \text{Prp}_{12} \ 11$)² and \pm calcite. The amphibole ranges in composition from mainly common magnesio-hornblende to magnesio-ferro-hornblende and pargasite (Leake et al., 1997; Hawthorne et al., 2012). Plagioclase in the ground-

* Supplementary data associated with this article can be found, in the online version, at doi: 10.7306/gq.1590

¹ Cores from the Rz 2 borehole are housed in the Carpathian Branch, PGI-NRI, Kraków, Poland. Cores from other boreholes that drilled the basement rocks in the horst are no longer available.

² Abbreviations of mineral names after Whitney and Evans (2010).

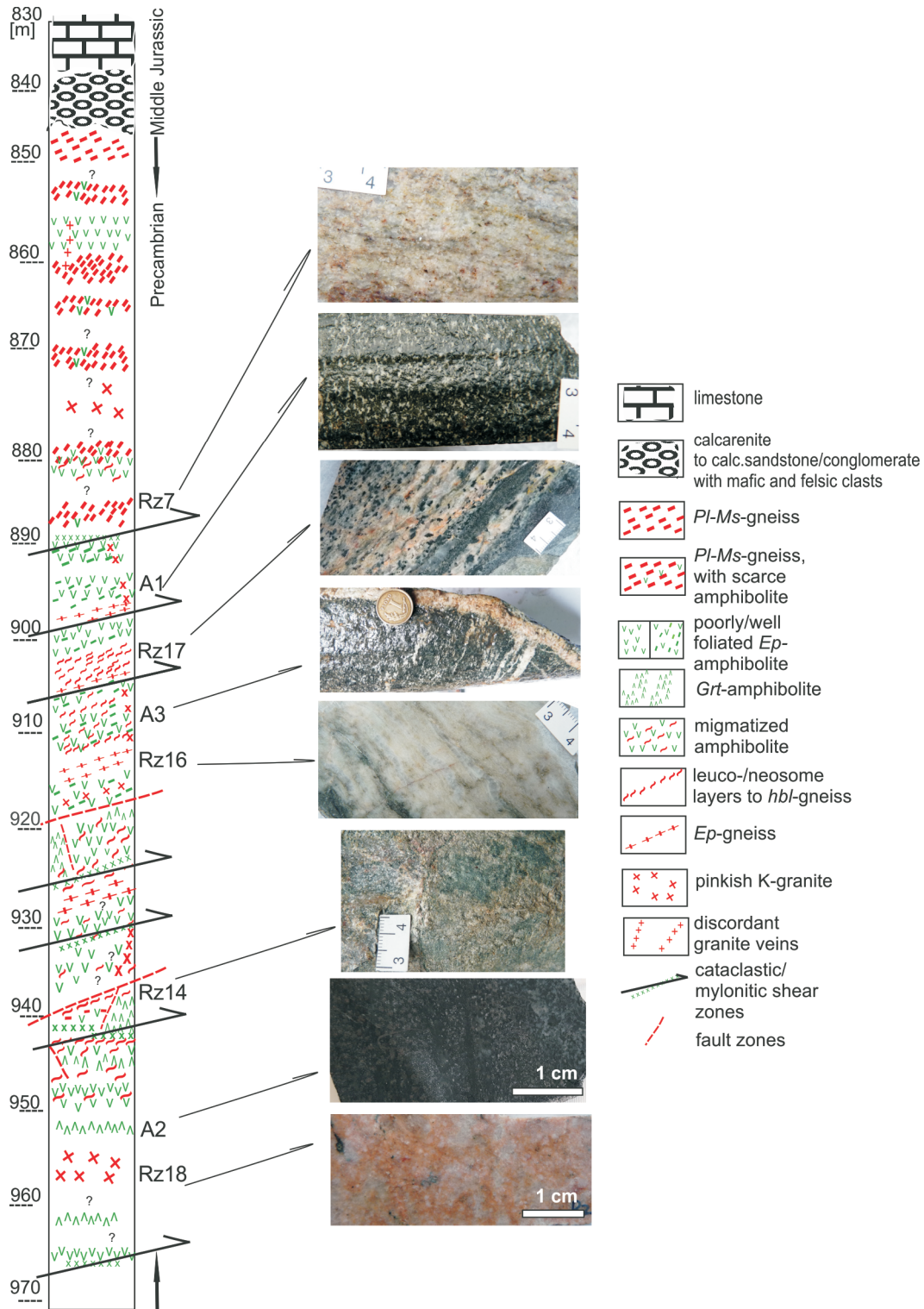


Fig. 2. Reconstructed lithologic log of the Rz 2 borehole

Sampled sites with pictures of the samples and location of thrust shears, cataclastic/mylonitic zones and normal faults are shown

mass is less calcic ($An_{17c} \ 5r$) than the plagioclase ($An_{22c} \ 11r$) included occasionally in the amphibole grains. While the cores of *Pl* grains contain abundant inclusions of randomly to directionally arranged epidote, the albitic rims are inclusion-free (Fig. 3B). In amphiboles, inclusions mainly of drop-like quartz and plagioclase, titanite, epidote and minor calcite are present. Calcite occasionally also occurs in the matrix, or forms veinlets accompanying retrograde shear zones.

Amphibolite type 2 (A2) occurs mainly in the lower portion of the borehole (~920–965 m). In contrast to amphibolite type 1, this is a relatively fine-grained rock, presumably derived from basaltic protolith (Figs. 2 and 3C, D). As compared to A1, it is composed of similar Ca-amphibole ($Mg \ # = 0.64c \ 0.46r$, $Si^{4+} = 6.87c \ 6.61r$), plagioclase (An_{20-10} , small groundmass grains: An_{6-3}) and abundant garnet ($Alm_{55c} \ 59r$ - $Grs_{23c} \ 20r$ - $Prp_{18c} \ 16r$), with significantly scarcer epidote, titanite and \pm cal-

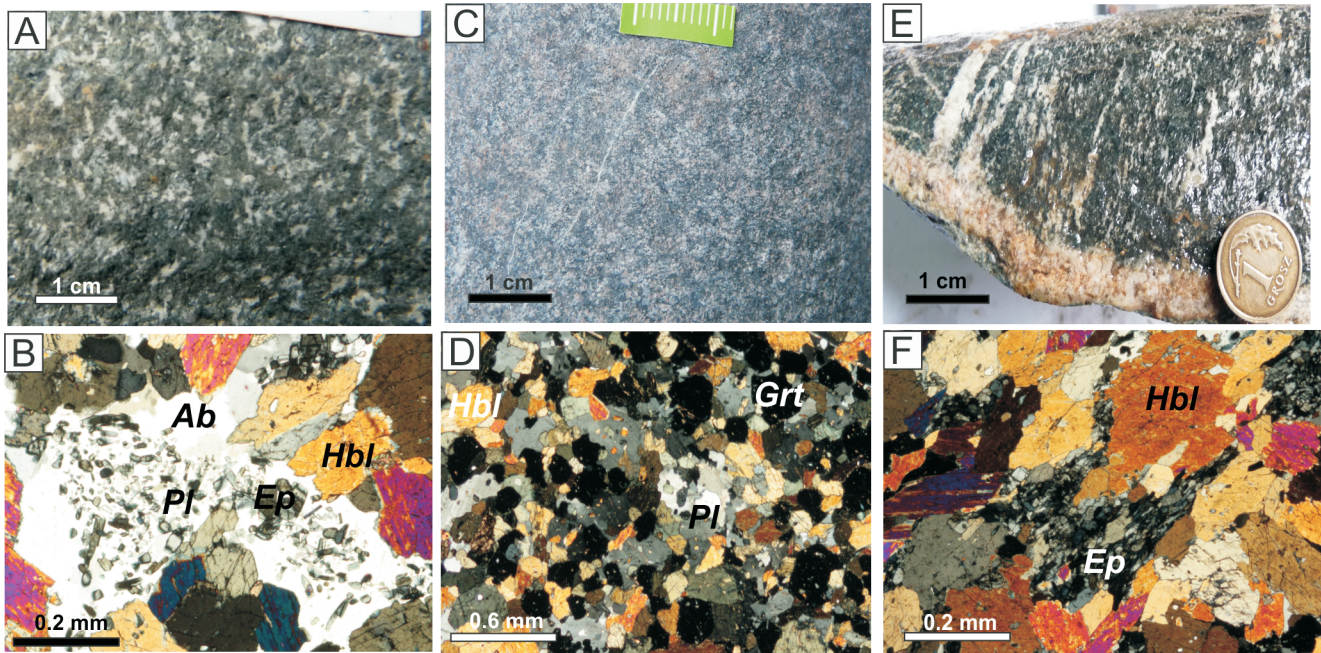


Fig. 3. Mafic rocks in the Rz 2 borehole

A, B – amphibolite A1; C, D – amphibolite A2; E, F – amphibolite A3; B, D and F – crossed polarizers; Ab – albite, Ep – epidote, Grt – garnet, Hbl – hornblende, Pl – plagioclase

cite. The amphibole classifies as Mg-Fe-hornblende to pargasite (Leake et al., 1997; Hawthorne et al., 2012). Larger oligoclase grains are embayed or intergrown with quartz and in the cores contain inclusions of epidote (Ps_{20-14}), drop-like quartz, hornblende and garnet.

In one sample of amphibolite type 2, magnesio-ferro-hornblende (ferro-hornblende, magnesio-hornblende, pargasite) and albite (An_{6-3}) are accompanied by epidote of bimodal composition ($Ps_{20-14, 4-3}$) and reversely zoned garnet ($Alm_{61c 54r-GrS_{21c 29r-Prp_{9c 15r}}$). Furthermore, in the Mg-hornblende, there are some lighter spots whose composition classifies them as ferrosadanagaite ($Mg\# = 0.004-0.007$, $Si^{4+} = 5.66$, $(Na+K)_A = 0.36-0.37$) and pale greenish rims of actinolite and ferro-actinolite ($Mg\# = 0.48-0.53$, $Si^{4+} = 7.35-7.53$, $(Na+K)_A = 0.14-0.24$) in the classification of Leake et al. (1997) and Hawthorne et al. (2012).

Amphibolites of type 3 (A3) are mesoscopically distinguished by the presence of felsic streaks and stripes that appear in a rock groundmass similar to amphibolite type 1 (Figs. 2, 3 E, F and 5E; Żelaźniewicz and Fanning, 2020: fig. 5). Striping zonally develops into more or less regular planar syntectonic layers (Fig. 5A), composed mainly of commonly elongated plagioclase porphyroblasts (with Hbl, Grt, Ep, Ms, Qz inclusions) associated with quartz, the two being variously accompanied by large epidote prisms, oblate epidote aggregates, amphibole blasts, white mica flakes and garnet (Fig. 3F). Such features appear as foliation-parallel leucosome/neosome portions which define a migmatitic character in the A3 amphibolites and may eventually enlarge to form up to several cm-thick bands of hornblende gneiss with sharp of diffuse interface against mafic mesosome, palaeosome or melanosome (Figs. 5A, E, F and 6A, B).

FELSIC ROCKS

The felsic rocks are represented by: plagioclase-muscovite gneisses, epidote gneisses, pinkish granites and leucoso-

mes/neosomes and hornblende gneisses in migmatized domains. They differ from one another in their mineralogy, fabric and varied proportions of the rock-forming and accessory minerals.

Plagioclase-muscovite gneisses (PI-Ms-gneiss), predominant in the upper portion of the drilled interval (Figs. 2 and 4A, B), are composed of plagioclase ($An_{12c 3r}$) and quartz with subordinate phengitic muscovite ($Si\ apfu = 3.17c 3.27r$), minor calcite and rare epidote (Ps_{14-15}). Minor alkali feldspar with a low Na-component ($Or_{96-97-Ab_{4-3}}$) and Kfs (Or_{100}) are present, mainly as thin films along the margins of subpolygonal quartz grains in PI-Qz layers. Rarely observed aggregates of fine-grained phengitic muscovite ($Si\ apfu = 3.3$) and K-feldspar replace an Al_2SiO_5 (kyanite? andalusite?) polymorph (Fig. 4C). Hornblende and garnet are very rarely present. Both may locally show chloritization.

In the drilled interval, epidote gneisses (Ep-gneiss) appear as sheared bodies within A1 and A3 amphibolites. Plagioclase ($An_{13c 6r}$) and quartz are accompanied abundantly by epidote and white mica and sparsely by K-feldspar, calcite, garnet, rutile, titanite and hornblende (Figs. 2 and 4D-F). Plagioclase is characteristically poikiloblastic with preferentially arranged epidote prisms (unzoned or $Ps_{7c 3r}$) inclusions which are parallel to those in the groundmass. Albitic rims are free of inclusions, which resembles the relationships observed in the A1 amphibolites. Phengitic mica (Si contents $apfu = 3.16c 3.37r$) and garnet ($Alm_{54-56-GrS_{25-30-Prp_{18-11}}$) are also compositionally similar to those in amphibolite type A1.

In contrast, the pinkish granite is an unfoliated rock composed of K-feldspar ($Or_{70-93} Ab_{28-5} An_{2-1}$), albite (An_{5-1}) and white mica ($Si\ apfu = 3.25-3.27$ in matrix and $3.30-3.34$ where included in feldspars; Fig. 4G-I). Relicts of Ca-poor pyrope-almandine garnet ($Alm_{60-61} Prp_{32-35} Grs_{2-5}$), rare apatite and allanite occasionally form large, densely packed aggregates (Fig. 4I). Epidote is very scarce or absent. In the alkali feldspar, there is a distinct tendency to increase the K-compo-

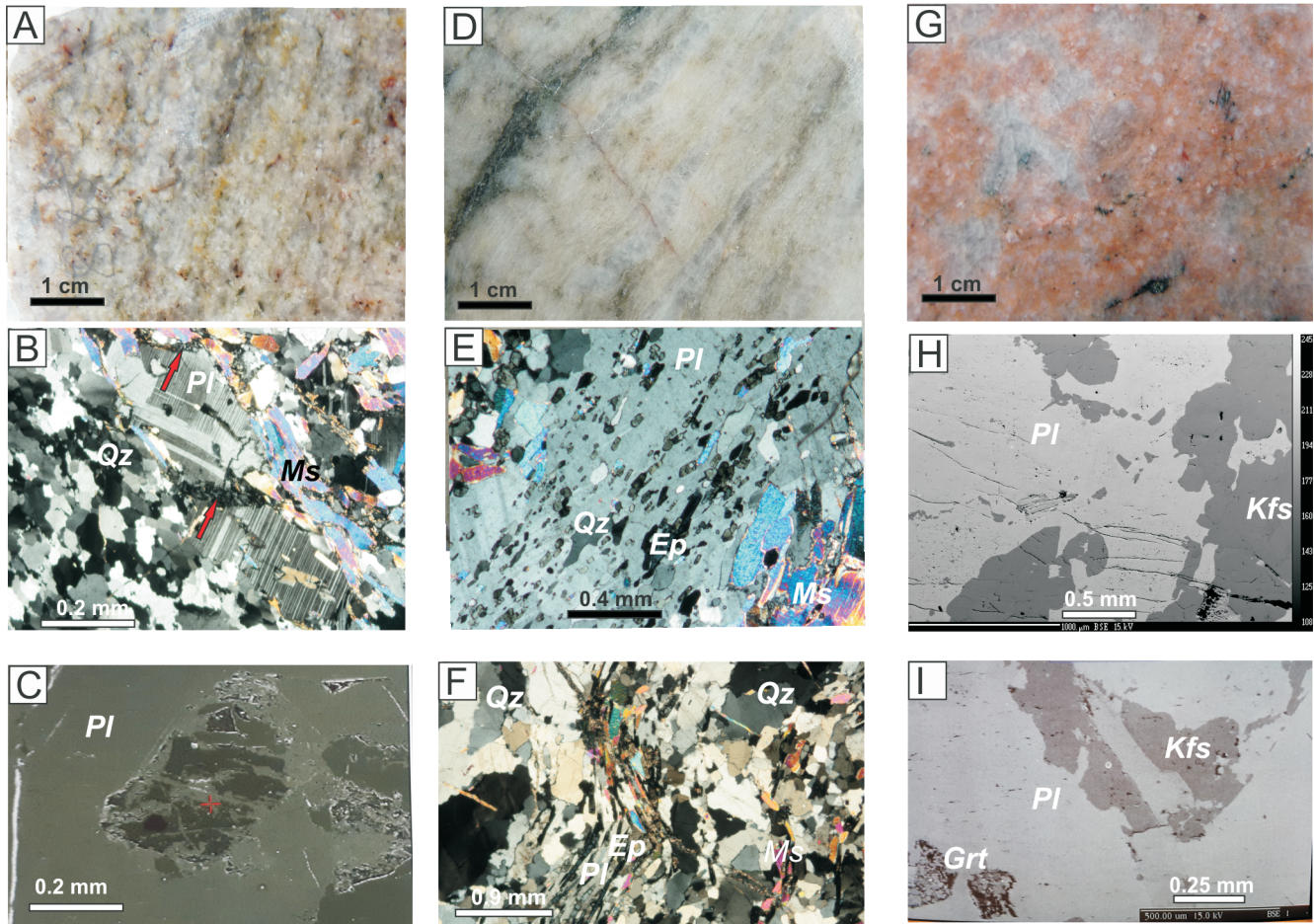


Fig. 4. Felsic rocks in the Rz 2 borehole

A–C – *PI-Ms*-gneiss: B – segregation of *Qz* and *PI-Ms* layers, fine-grained crystallized *Qz-Ab-Kfs* partial melt, C – relict Al_2SiO_5 phase in *PI* grain; D–F – *Ep*-gneiss: E – *PI* with preferential orientated *Ep* and *Qz* inclusions, F – syntectonic segregation of *Qz* and *PI-Ep-Ms* layers; G–I – pinkish K-granite: H – intergrowths of *PI* and *Kfs*, I – *Kfs* at boundaries of *PI* grains, relic *Mg-Grt*; B, D, H – crossed polars; F, G, I – BSE images; *Kfs* – K-feldspar, *Ms* – muscovite, *Qz* – quartz, other explanations as in Figure 3

ment and decrease the Na-component toward the rims of grains with highly irregular shapes. K-feldspar, that forms embayments or extensively replaces albite, also appears as inclusions in phengite and in albite, and develops intergrowths with quartz (Fig. 4H, I). In the Rzeszotary K-granite, K-feldspar itself may contain albite, mica and quartz as inclusions.

Neosomes in the migmatized domains are widely diverse (Fig. 5A–J). Cross-cutting veins are clearly injections (Figs. 3E and 6D), either mainly quartzofeldspathic or similar to pinkish K-granite yet with \pm some admixtures of hornblende and plagioclase. More common are layers and segregations or veins parallel to the foliation in the host rocks. Some are also granitic injections; most of them are not. In the felsic gneisses, leucosomes of variable grain size are composed of coarse quartz, feldspars (*PI*, *Ab* \pm *Kfs*) and white micas. They alternate with a mesosome comprising marked concentrations of plagioclase and a variety of minerals that characterize a given gneiss type (Fig. 5). Such migmatitic segregations were penetrated by alkali feldspars, identifiable in split micas, thin films on plagioclase grains, or in sealed microfractures (Figs. 5I and 6G).

Coarse-grained hornblende gneisses stem from thickened *PI-Qz* neosome with increased contents of *Hbl* (Figs. 2 and 5C, D), accompanied by *Ms* \pm *Grt*, *Kfs*, *Ttn/Ilm*, *Chl*, *Cal*. In neosome bands up to several centimetres thick, alternations of light and dark zones are developed. The latter mainly comprise

Hbl-Grt-Ms, the former are composed of quartz and poikilitic plagioclase grains accompanied by single hornblende grains riddled with mainly *Qz* inclusions (Fig. 5D).

In some fault zones (~942–940 m, ~965 m), a coarse-grained *Hbl*-granodiorite patchily appears (Figs. 2 and 5H). This consists of inversely zoned plagioclase (An_{40-18r}), quartz, large flakes of phengite ($\text{Si apfu} = 3.42c \text{ } 3.32r$), alkali-feldspar ($\text{Or}_{96c} \text{ } 97r \text{ } \text{Ab}_{3 \text{ } 2}$), epidote ($\text{Ps}_{18c} \text{ } 20r$), garnet ($\text{Alm}_{60c} \text{ } 45r \text{ } \text{GrS}_{30c} \text{ } 45r \text{ } \text{Prp}_{5 \text{ } 9}$) and Mg-hornblende.

COMPOSITIONAL ZONATION OF THE MINERALS

As indicated above, in both mafic and felsic rocks, compositional zoning was commonly observed in the rock-forming and accessory minerals. In plagioclase grains, oligoclase cores are discretely overgrown by albite ($\text{An}_{22c} \text{ } 5r$). The oligoclase cores often enclose epidote (Ps_{20-14}) inclusions that are absent from the albite rims. In amphibole grains, epidote inclusions are also confined only to the host cores. Low-An albite grains do not enclose epidote either. In low-Fe epidote grains, Fe^{3+} contents tend to decrease from core to rim ($\text{Ps}_6 \text{ } 4$). Most garnet grains display increasing Fe but decreasing Ca and Mg contents towards the rims. Amphibole grains also enclose drop-like quartz inclusions. All these features record the trend of metamorphic transformations on a retrograde path.

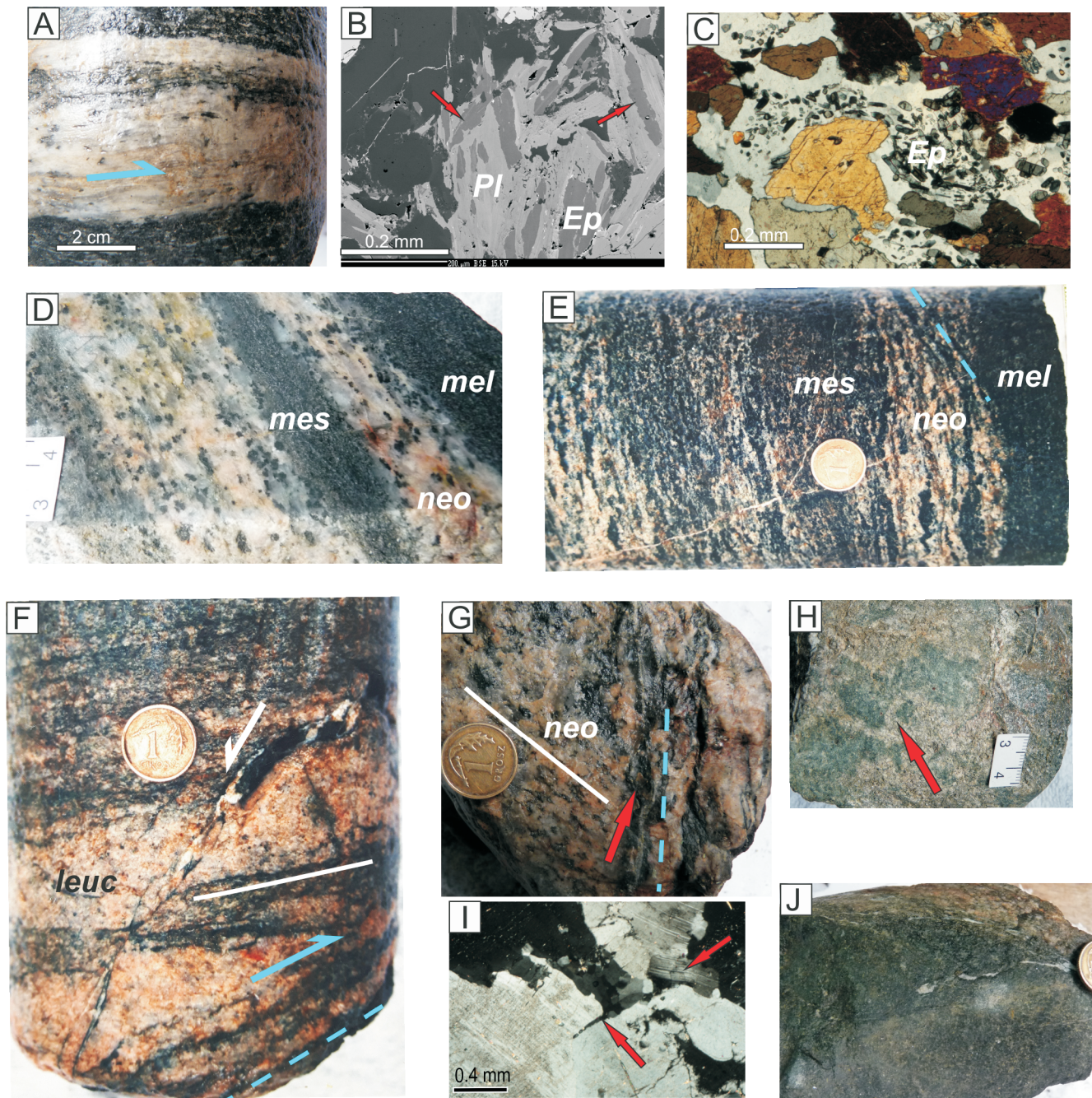


Fig. 5. Examples of tectonic deformation

A – shearing localized in *Ep*-gneiss, quartz ribbons and small fold indicate the sense of thrust movement (blue arrow); **B** – BSE image of syn-shear fold of a plagioclase grain (*Pl*) with folded epidote inclusions (darker grey shown by *Ep* and red arrows); **C** – plagioclase grains with parallel-oriented epidote inclusions syntectonically bent and wrapped around more rigid *Mg*-hornblende grains, crossed polars; **D** – foliated migmatite, note preferred orientation of large amphibole, plagioclase and ribboned quartz grains in the neosome turning to *Hbl*-gneiss; **E** – strongly foliated amphibolite migmatized by segregation/differentiation with sheared neosome (blue dashes); **F** – sequence of deformation: in striped amphibolite A3, migmatitic leucosome that developed parallel to the foliation (white line) became then obliquely sheared (blue dashes) during thrusting (blue arrow) and overprinted by extensional faulting (white arrow), note quartz (and calcite) veinlets in the fault zone; **G** – gently foliated neosome (white line) intersected by oblique shear zone (blue, red arrow); **H** – brecciated portion of amphibolite A2 (arrow) cemented with *Hbl*-granodiorite (lighter), feasible effects of hydraulic-fracturing during granitoid intrusion; **I** – rigid behavior of plagioclase grain with bent twin lamellae and fractures/fissures (arrows) healed with *Kfs*; **J** – breccia with various amphibolite lumps, quartz veinlets in the middle lump parallel to its borders; leuc – leucosome, mel – melanosome, mes – mesosome, neo – neosome; other explanations as in Figure 3

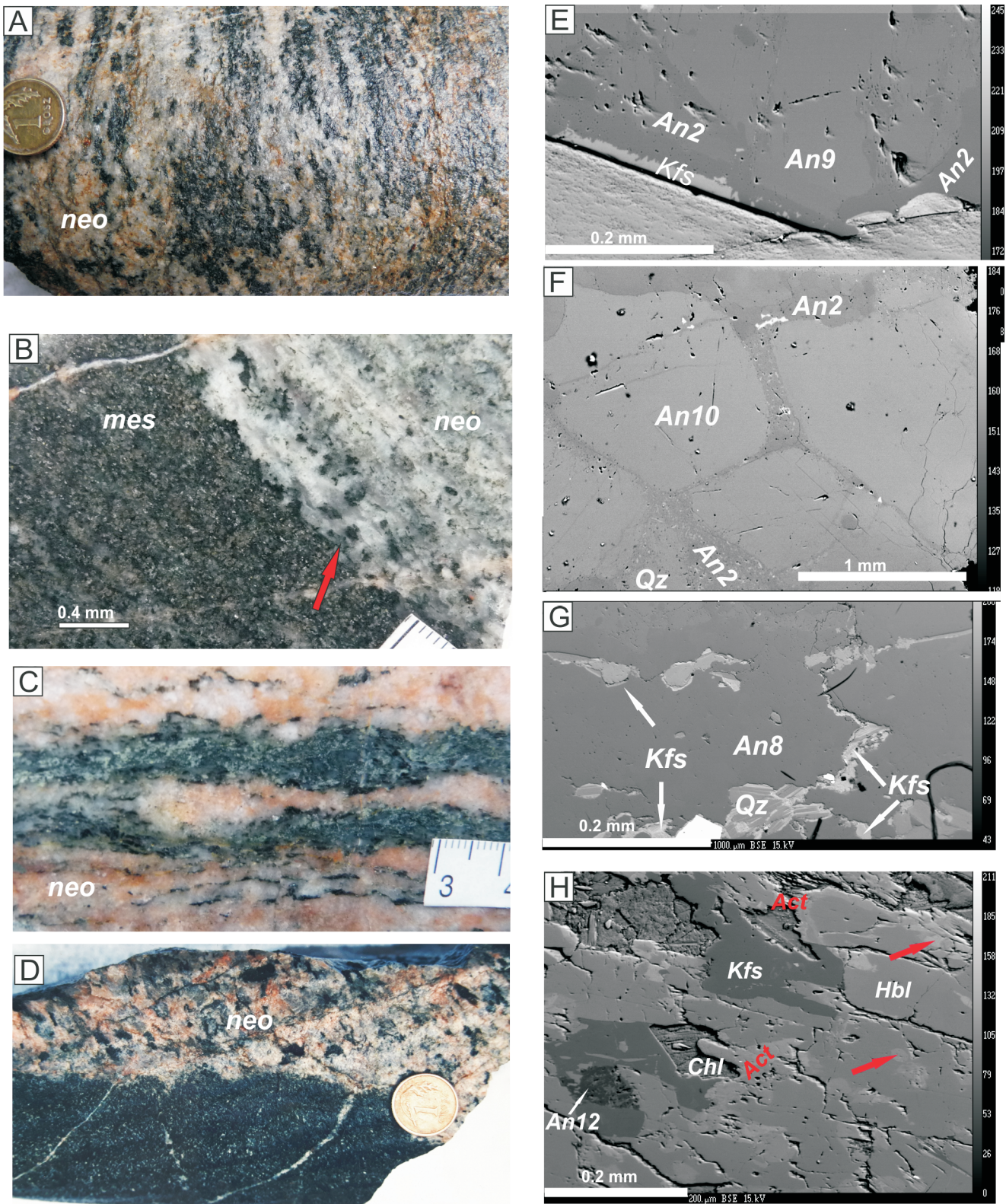


Fig. 6. Records of migmatization

A – amphibolite A3 migmatized by syntectonic fluid-assisted segregation; **B** – mesosome-neosome interface (arrow) with large grains of quartz and poikilitic hornblende and plagioclase pointing to the importance of fluid assistance; **C** – advanced stage of neosome formation resulting in alternation of *Qz-Ab* domains and *Pl-Hbl-Qz-Ms* layers with mimetically retained foliation; **D** – oblique injection of granitic neosome in almost undeformed amphibolite A1; **E** – plagioclase rimmed by albite with later *Kfs* seam at the straight border with mica; **F** – in plagioclase segregation, albite films separate texturally equilibrated polygonal *Pl* grains with like-like contacts; **G** – *Qz-Kfs* seam developed between plagioclase grains, inter- and intragranular penetration of *Kfs* in *Pl*, including at borders with *Qz* inclusions; **H** – magnesio-hornblende (*Hbl*) rimmed and along fractures (arrows) replaced by actinolite (*Act*), alkali fluid activity shown by K-feldspar (*Kfs*), chlorite (*Chl*) and decayed plagioclase (*An12*); E–H – BSE images; other explanations as in [Figure 5](#)

DEFORMATION AND METAMORPHISM/MIGMATIZATION

TECTONIC DEFORMATION

The Rzeszotary rocks, except for the granites, were more or less affected by synmetamorphic deformation. In *Pl*-*Ms*-gneisses, foliation is expressed by mica flakes, plagioclase (*Pl*>>*Qz*) and quartz (*Qz*>>*Pl*) layers/ribbons that alternate zonally (Fig. 4B). In *Ep*-gneisses, the felsic layers and quartz ribbons alternate with polymineralic *Pl*-*Ms*-*Ep* ± *Grt* layers (Fig. 4F). In the latter, flattened plagioclase grains contain abundant epidote inclusions parallel to epidote (*S₁*/*S_e*) and muscovite flakes in the matrix (Fig. 4C, D). Amphibolites are generally less foliated, this depending on the degree of the preferential orientation of plagioclase and amphibole blasts and occasional white micas (Fig. 3).

In the Rz 2 log, shear zones appear several times (Figs. 2 and 5A, E, F). The shear strain was preferentially localized in the rheologically weaker felsic rocks, *Ep*-gneisses in particular (Fig. 5A). Synmetamorphic deformation and recrystallization is documented by mica fishes, folded micas overgrown by plagioclase (Fig. 5B) and elongate plagioclase blasts occasionally bent against more rigid amphibole grains (Figs. 4D and 5C). In migmatized amphibolites, elongate/oblate aggregates of parallel-oriented epidote prisms set amidst the amphibole grains contribute to the foliation and so do hornblende prisms in the strained neosome *Hbl*-gneiss (Figs. 3F, 5D and 6C).

Mineral lineation seen on the foliation planes points to mainly dip-parallel kinematics. There are records of multiple shear episodes. The earliest recognizable ductile shearing had a reverse sense of movement (Fig. 5A) on planes that dip at an angle of 0–35° (to the core axis), being parallel or oblique to the foliation. The varying attitude of the latter suggests folding which together with thrusting and occasional small-scale intrafolial folds indicate shortening and contractional tectonics. Despite obvious disjunctions and sliding, the sense of tectonic transport is not always determinable (Fig. 5F, G). However, ductile (thrust) shearing clearly preceded later more brittle deformation that occurred in an extensional normal regime (Fig. 5F, G; Żelaźniewicz and Fanning, 2020: fig. 5). As the borehole cores have not been oriented (except for the top-bottom orientation), the observed kinematics cannot be related to geographic coordinates.

In the gneisses, synmetamorphic tectonic deformation produced a fabric and lensoid segregations of felsic minerals (*Qz* and *Pl*-*Qz* layers) with records of grain boundary migration (GBM), recrystallization at relatively high temperature and later bulging (BLG) at lower temperatures, which indicates dynamic recrystallization. In the epidote gneiss, linear dispersion of accessory minerals (*Grt*, *Ep*) within polymineralic layers (*Pl*-*Ms*-*Ep*-*Bt*+*Grt*) are evidence of high shear strain. In the strain zones, epidote and white mica (re)crystallized as secondary minerals.

In migmatized felsic gneisses, films and veinlets of alkali feldspar (*Or*_{97–96} *Ab*_{3–4}) appear along the plagioclase grain borders and in fracture networks inside the grains (Fig. 6E–G). Fracturing, breakage and bending of the twin lamellae point to a rigidity contrast between plagioclase on one hand and K-feldspar and quartz on the other. K-feldspar penetrated fractures

and space between displaced fragments of plagioclase grains (Figs. 5I and 6G).

These features developed in a contractional regime which also controlled the syntectonic metamorphism and migmatization (Fig. 5; Żelaźniewicz and Fanning, 2020: fig. 5). A subsequent extensional overprint, mainly under greenschist facies conditions, was reflected by narrow shear zones and a S-C' fabric. In amphibolites, such zones are variously emphasized by secondary chlorite and minute white micas, often accompanied by calcite, cataclastic comminution of amphibole grains and dynamic recrystallization of quartz.

Locally, fault zones/planes can be observed (~920 m, ~927 m, ~940 m; Fig. 2). A fault breccia of brittle fragmented amphibolite, found in one of the fault zones (depth of 940 m), was specifically cemented with a granitic mass (*Grt*-*Ep* granite to *Hbl*-granodiorite), resembling products of hydraulic fracturing (Fig. 5H). Another piece of breccia contains different rocks stuck together: neosome and two kinds of amphibolite (Fig. 5J). The scarcity of borehole cores severely limited more detailed observations.

Considering the presence of several shear zones (Fig. 2) in the interval drilled, it cannot be excluded, or demonstrated, that in the drilled interval, the upper, mainly gneissic domain and the lower, mainly metabasitic domain have been structurally juxtaposed by the thrusting which took place within the Rzeszotary complex. At a small scale, tectonic (shear) contacts between rheologically different rocks were observed in the borehole cores (Fig. 5A, E–G).

METAMORPHISM/MIGMATIZATION

In general, mineral compositions of the Rzeszotary rocks described above and (micro)structural records indicate syntectonic metamorphism under epidote amphibolite facies conditions (Figs. 3 and 4). Migmatization³ affected both gneisses and amphibolites. The latter range from streaky/striped variants to stromatic migmatite (Fig. 6A–C) with occasional melanosomes (Fig. 5D; Żelaźniewicz and Fanning, 2020: fig. 5). In amphibolites A3, a *Qz*-*Pl*-*Ab*-*Kfs* neosome developed with large blasts of quartz, and amphibole and plagioclase, both sieve-textured, in particular at the interface with mesosomes (Fig. 6B). Such large *Hbl* and *Pl* blasts enclose *Qz*, *Grt* and *Ep* inclusions. There are subordinately phengite (*Si* apfu = 3.2_c 3.4_r), corroded garnet (*Alm*_{55c} *58r* *Grs*_{27c} *30r* *Prp*_{16c} *11r*) and ± epidote (*Ps*_{7c} *5r*) crystals. Albite (*An*_{10c} *2r*) is zoned inversely and coexists with Ca-rich garnet.

Common signs of migmatization (Fig. 6) point to relatively high temperatures whereas large white mica flakes that grew on the foliation planes in migmatized domains suggest fluid activity. Microscopic/mesoscopic evidence and mineral compositions of neosomes suggest that apparently H₂O and CO₂ volatiles, alkali fluids and partial melting must have been jointly in operation.

In migmatized *Pl*-*Ms* gneisses, some neosome layers are almost monomineralic concentrations of plagioclase grains with subpolygonal boundaries decorated by thin films of alkali feldspar (*Kfs*+*Ab*, *Kfs* or *Ab*) and dispersed opaque impurities (Fig. 6E, F). Prior to such decoration, plagioclase grains in these concentrations had like-like boundaries (Ashworth and McLellan, 1985), characteristic of metamorphic differentiation

³ The descriptive terminology of migmatites (Mehnert, 1968; Ashworth, 1985) has been used. In the Rzeszotary case not only partial melting, inherent in genetic classification (Sawyer, 2008), was in operation.

that operated in the course of migmatization. *Kfs* ($\text{Or}_{98-96}\text{Ab}_2\text{An}_{2-0}$) spread as veinlets along fractures (Figs. 5I and 6E, G) and forms its own anhedral grains. It also occurs as overgrowths on Ca-richer plagioclase grains, corrodes and replaces both quartz and plagioclase or appears inside them. Such ubiquitous presence of alkali feldspars indicates inter/intra-granular circulation of fluids. The albite films on plagioclase grains (Fig. 6F) or as a fine-grained *Qz-Ab-Kfs* phase that crystallized in interstitial and extensional spaces between grains (Fig. 4B) may suggest partial melting.

All those features, including the increased yet bimodal grain size in neosomes, the presence of melanosomes as well as alternations of layers rich in quartz and feldspars with layers rich in amphibole and plagioclase (Figs. 5D and 6B, C) or with layers dominated by *Grt*, *Ms*, *Ep* \pm *Ttn*, *Cal*, may have developed due to metamorphic segregation assisted by fluids, to partial melting, or to concurrent operation of the two mechanisms. Such an option seems suggested by the mineral compositions observed in neosomes/mesosomes and by the microstructural evidence noted above.

Whatever the case, migmatization took place with influx of not only H_2O but also of CO_2 as suggested by the occasional presence of accessory calcite in the mineral framework. Microscopic observations show that zones of ductile shearing channelized fluids/liquids which effectively promoted that process.

The K-carrying fluids or partial melts may have been genetically connected with the same crustal source that provided K-rich ($\text{K}_2\text{O} > 8$ wt.%) pinkish granite. Some K-granite intervals that occur at the upper and lower sectors of the borehole log (Fig. 2) may have represented apophyses from a larger more deeply-seated magma body that also likely sourced granitic neosome veins observed in the migmatized portions of the drilled interval of the Rzeszotary 2 borehole.

P-T CONDITIONS

Despite chemical and structural differences, the A1–A3 amphibolites did not differ qualitatively in mineral compositions, yet variations in chemical compositions (cores and rims) of mineral phases in direct contact enabled classic thermobarometric calculations. Assessments of *P-T* conditions of metamorphism were somewhat hampered as most geothermobarometers have been calibrated for igneous systems. However, Holland and Blundy (1994) introduced the amphibole–plagioclase thermometer with a strong thermodynamic basis, calibrated for both igneous and metamorphic assemblages. This was utilized to estimate temperature for five samples of the Rzeszotary amphibolites (two A1, two A2 and A3). Pressure conditions were approximately assessed by means of the Al-in-hornblende barometer using calibrations for igneous rocks made by Hammarstrom and Zen (1986) and Schmidt (1992). The former provided lower values by ~ 0.2 – 0.4 kbar as compared to the latter and both yielded two clusters: 8.0–8.9 kbar and 5.2–6.9 kbar. No systematic relation was observed to the temperature assessed by the Holland and Blundy (1994) thermometer (reaction: edenite+4 quartz=tremolite+albite) within the range of 575–640°C. Temperatures of $< 600^\circ\text{C}$ were obtained using the experimental geothermobarometer of Plyusnina (1982) for pressures of 9–10 kbar. Notably, the *Hbl-Pl* thermometer of Blundy and Holland (1990) gave markedly higher values for the same pairs analysed. These results are roughly systematically ordered and similar throughout the vertical borehole profile (Fig. 2). The pairs of host amphibole cores and plagioclase (An_{22-17}) inclusions yielded *P-T* conditions of 655–625°C/8.5–9.0 kbar whereas in the matrix the pairs of *Amp*

cores and *Pl* cores (An_{10-11}) yielded *P-T* of 580–550°C/9–10 kbar and 565–490°C/8.5–5.2 kbar for the *Hbl* rim-*Pl*(An_{7-3}) rim pairs. Evidently, the less the An content, the lower the temperature estimate. On the other hand, the garnet-hornblende geothermometer (Ravna, 2000), calibrated for basaltic and semipelitic rocks, gave temperatures of 550–580°C for the A2 amphibolites, similar to other results, but only 370–460°C in the A1 amphibolites, which is however unrealistically low.

Thermodynamic modelling (*THERMOCALC* 3.33) gave more insight into the *P-T* conditions of metamorphic transformations of the amphibolites studied, and constrained the above results. The chosen *P-T* space in both samples ranges from 4 to 13 kbar and 450 to 750°C. The *P-T* diagram has been contoured with specific compositional isopleths of *Hbl*, *Pl*, *Ep* and *Grt* that are $X(\text{Hbl}) = \text{Fe}/(\text{Fe}+\text{Mg})\times 100$, $\text{Ca}(\text{Pl}) = \text{Ca}/(\text{Ca}+\text{Na})\times 100$, $\text{F}(\text{Ep}) = \text{Fe}^{3+}/(\text{Fe}^{3+}+\text{Al})\times 100$, $X(\text{Grt}) = \text{Fe}^{2+}/(\text{Fe}^{2+}+\text{Mg})\times 100$ and $Z(\text{Grt}) = \text{Ca}/(\text{Ca}+\text{Fe}^{2+}+\text{Mg})\times 100$.

In the calculated phase diagram for A1 amphibolite, the dominant mineral assemblage matched the field of *Hbl-Ep-Pl-Spn-Qz-Act-H₂O* (Fig. 7A, pseudosection A1). This mineral assemblage was stable within a range of 500–560°C and 6.2 and 10.2 kbar. Within this range, intersections of compositional isopleths of *Ca(Pl)*, *X(Hbl)* and *F(Ep)* obtained from cores of these minerals indicate conditions close to 7–8 kbar and 520–550°C. The increasing *X(Hbl)* and decreasing *Ca(Pl)* values, furthermore, indicate retrogression related to decrease of temperature below 450°C (Fig. 7A, pseudosection A1). Such results of thermodynamic modeling are generally in line with microscopic observations and the classic exchange geothermobarometry mentioned above, which utilized the chemical compositions of the *Pl* and *Hbl* grains in direct contact. However sample A1 contains subordinate garnet that was not considered in the classic thermobarometric calculations based on hornblende and plagioclase. For the bulk composition studied, this garnet was stable at temperatures exceeding 650°C and pressures exceeding 10 kbar, hence under *P-T* conditions somewhat higher than those deduced from the conventional thermobarometry. It is possible that garnet developed in A1 amphibolite mainly under such slightly higher conditions and a little earlier than the stage of the metamorphic evolution that was recorded by the plagioclase inclusions in amphibole and by the host amphibole cores. This preceded further recrystallization of amphibole and plagioclase in the matrix at decreasing pressure and temperature. Nevertheless, a lack of equilibrium between garnet and other phases cannot be entirely ruled out.

The calculated *P-T* diagram for sample A2 indicates that quartz and garnet are more stable, while epidote is less stable than in sample A1 (Fig. 7B, pseudosection A2). This matches the mineral compositions of both amphibolites. A2 contains abundant garnet and minor epidote, whereas A1 has minor garnet but abundant epidote. Nevertheless, the mineral isopleths of the three dominating phases – *Pl* (core compositions), *Hbl* (core compositions) and *Grt* (core and rim compositions) – intersect at conditions of 11–12 kbar and temperatures of ~ 650 – 700°C , in the fields that also embrace *Qz*, *Di* and *Rt* ($\pm \text{Ilm}$). *Rt* and *Di* are absent from the rocks, which suggests that these phases may have been removed during later retrogression, hence they were not seen in the thin sections. On the other hand, products of such retrograde reactions might not be easily identifiable in the rocks studied. In any event, the calculated *P-T* conditions (peak *T* at $\sim 700^\circ\text{C}$) for A1 and A2 were also able to trigger migmatization of rocks of the Rzeszotary complex, in particular under the ‘wet’ conditions inferred and decompression.

The conditions modeled are considered to indicate the temperature peak. The prograde part of the P - T path can be reconstructed only partially. The prograde mineral assemblage included epidote, which is minor and occurs as inclusions in the cores of oligoclase grains, while it is missing from low-An albite grains. The prograde part of the P - T path can be thus correlated with a change in P - T conditions under which epidote was no longer stable and the main phases in sample A2, i.e. *Grt-Hbl-Pl*, began to dominate due to the temperature rise. Accordingly, the P - T diagram calculated shows that the P - T path must have crossed the *Hbl-Pl-Ep-Spn-Qz-Grt* field, which is stable within a relatively narrow range of 10.2–11.4 kbar and 580–600°C (Fig. 7B). Similarly to A1, microstructural relationships between oligoclase cores and albite rims in sample A2 indicate retrogression. In the amphibolites (also in the *Ep*-gneisses), the lack of epidote inclusions in albite rims (Fig. 3B) suggests that Ca was effectively partitioned in epidote and plagioclase cores during earlier stage(s) of common metamorphic transformations.

Although the P - T conditions were mainly assessed and calculated for the mafic rocks, they may be safely extended to the felsic rocks as the two lithologies were intimately connected during metamorphism. The thermodynamic modeling of samples A1 and A2 fully supports the view that the Rzeszotary complex underwent metamorphism at temperatures high enough to promote incipient partial melting in the presence of fluids, in particular in its felsic member. The results of thermodynamic modeling are generally in line with 'classical' thermobarometric calculations, the compositional zonation of the minerals and microscopic observations that together documented the (post?) peak and retrograde part of a clockwise P - T path.

Faint indications of earlier higher P - T conditions have also been observed in the Rzeszotary rocks. In one of the amphibolite A2 samples, some Mg-hornblende grains enclose low-silicic and almost Mg-free traces of sadangaite. If these are relicts(?) then together with the nearby garnet (Fe contents decreasing and Mg and Ca increasing towards the rims) this would suggest metamorphism at higher pressures. Provided the *Al-in-Hrb* barometer was applicable in such a case, a pressure of ~17–19 kbar would be reached. Another suspect object is an Al_2SiO_5 phase (kyanite? andalusite?) found in *Ms-Pl*-gneiss, which was pseudomorphed and partly replaced with an aggregate of Fe-phengite, quartz and K-feldspar (Fig. 4C). Yet another suspect trace of an earlier higher pressure episode in the evolution of the Rzeszotary complex takes the form of a few Mg-rich but Ca-poor garnets in the 2.0 Ga K-granite (Żelaźniewicz and Fanning, 2020).

GEOCHEMISTRY

Eight samples were selected for whole-rock major element and trace element analyses. Representatives of each of the rock types described above were analysed (Appendix 1). The geochemical characters of three type of amphibolite, four types of felsic rock and the *Hbl*-granodiorite were assessed. In the migmatized amphibolite, the mafic palaeosome (mesosome) was analysed for amphibolite type 3 and a leucocratic layer for neosome. For four samples, Sm-Nd isotopic compositions and abundances were measured.

MAFIC ROCKS

The petrographic differences noted above between the Rzeszotary amphibolites are to some extent also observed in their geochemistry (Appendix 1). A limited number of samples available for analyses do not permit deciphering of systematic

variations and impeded considerations of their origin and genetic relationships. However, the differences noted allow for some patterns to be discriminated, as characterized below, and for a few speculative conclusions.

CLASSIFICATION

All of the Rzeszotary amphibolites (A1, A2, A3) fall within the tholeiitic field on the AMF and TAS diagrams (Fig. 8A, B, L) and classify as oceanic tholeiitic basalts with medium K and relatively high Al_2O_3 contents (Appendix 1). However the three types differ as regards all other elemental abundances and characteristic ratios. They are metaluminous and subdivide into high-Mg tholeiite (A1, A3) and high-Fe tholeiite (A2) as indicated by a Al - Mg - $(Fe^{3+}+Ti)$ diagram (Fig. 8B), differ in the Mg# index: 52 in A1, 46 in A3 and 28 in A2, and thus also differ in FeO^*/MgO ratios. On the other hand, the SiO_2 contents of 46.8 wt.% in A1 is significantly lower than that of 51.7 wt.% in A2. Similar relationships are shown by TiO_2 , thus consequently in the SiO_2 - Zr/TiO_2 plot (Fig. 8C), A1 corresponds to an alkali basalt and A2 and A3 to subalkaline basalts, with A/CNK ratios of 0.6 and 0.7, respectively. In general, the elemental abundances in A3 are closer to those of A1 than A2, which is consistent with the observation that A3 is a migmatized variant of A1. Further characteristics will be given mainly for A1 and A2 as the two are markedly different types of the Rzeszotary metabasites.

GENETIC/GEOTECTONIC CHARACTERISTICS AND IMPLICATIONS

The above features indicate that the parent magma of A2 was more evolved than that of A1, as is also suggested by incompatible element ratios ($Zr/Hf = 34.6$ vs. 38, $Nb/Yb = 1.3$ vs. 1.9, $La/Gd = 1.4$ vs. 2.25) and by different abundances of transition elements (70 ppm Ni vs. 254 ppm Ni and 46 ppm Cr vs. 229 ppm Cr for A2 and A1, respectively). Furthermore, comparing A1 and A2, such ratios as Nb/U (60 vs. 27), Nb/Th (26 vs. 10.4), Th/U (2.3 vs. 1.1), or Th/Ce (0.01 vs. 1.1) also suggest a less evolved magma in the case of A1.

The Ti/V ratios (16.2–19.6) suggest that the metabasite parent magmas overlapped the IAT-MORB transition (Fig. 8E), whereas in the MnO - TiO_2 - P_2O_5 diagram and in the Zr - Ti/V and Zr - Y/Zr plots (Fig. 8D, F, G) they all fall in the arc fields. In the diagrams based on the immobile trace elements Th, Yb, Hf and Ta (Fig. 8I), the amphibolites A1 and A2 plot as MORB and IAT whereas A3 is in the field of within-plate tholeiites.

For the metamorphic rocks the trace elements are yet more important. The REE spider plot normalized to chondrite (Fig. 8J) shows almost no difference between A1 and A2. A3 shows slightly higher abundances of REE with enrichment in LREE, which probably may be attributed to migmatization and fluid influence on the amphibolitic mesosome (not noticed during microscopic examination).

In the trace and REE diagrams, element abundances normalized to N-MORB (Fig. 8K) are more variable. A3 is richer in LREE yet the three are significantly enriched in incompatible, fluid-mobile LIL elements (K, Ba, Rb, Cs) and transition metals (Pb, U). However, A1, as compared to A2 and A3, is markedly depleted in U, Th, Nb, though more abundant in Pb than A3. The overall composition of the three amphibolite types is similar to modern IAT/MORB (Fig. 8D–I), as they have tholeiitic basalt composition, enriched in LILE and depleted in HFSE with flat REE (A1 and A2) and $Gd_N/Yb_N < 2$. Though they fall in the arc fields on most plots (Fig. 8D–H), other petrogenetic diagrams indicate MORB mantle either for A1 or for all of them (Fig. 8I). However, in the Zr - Ti - Y discrimination plot, the three rocks locate in the ambiguous field B (Pearce, 1996). While Ti/Y ratios

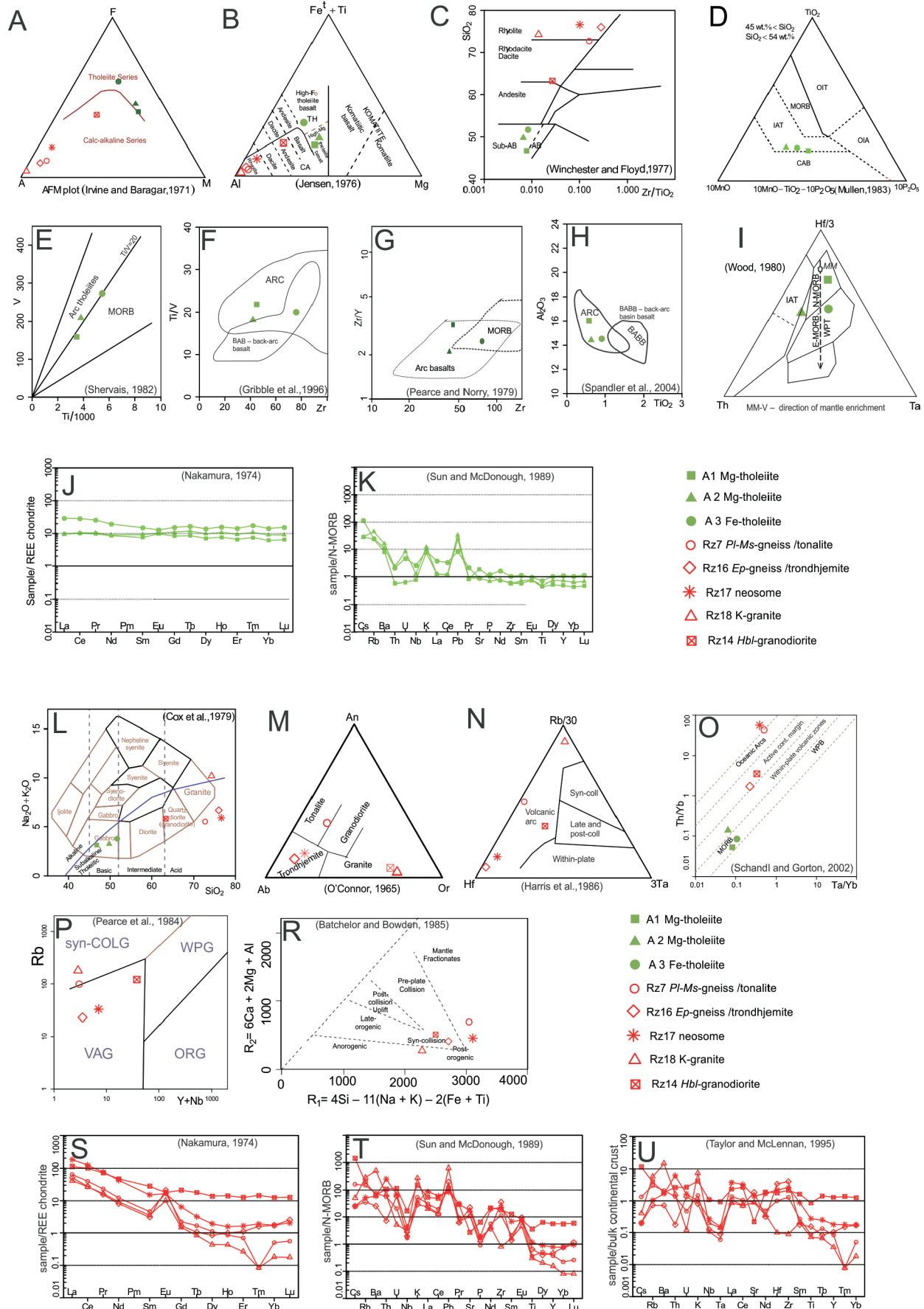


Fig. 8. Geochemistry of main rock types in the R2 zone borehole

A–C, L – classification diagrams; D–K – mafic rocks; M–U – felsic rocks; see text for details; CAB – continental basalt, IAT – island arc and volcanic arc tholeiite basalt, MORB – Mid-Ocean Ridge Basalt, OIA – oceanic alkaline island, OIT – oceanic island tholeiite basalt, WPB – within-plate basalt, WPT – within-plate tholeiite basalt

generally exclude WPB and garnet lherzolite melting and the lack of a Nb anomaly with respect to Th and Ce (Fig. 8K) does not concur with arc basalts, the Nb, Zr, Ti, Y abundances are below those of N-MORB and such absolute depletions are characteristic of IAT. On the other hand, the above characteristics along with low Nb, Ta, Th, Sr, P, Ti may have been due to a subduction-related island-arc setting and incipient melting of dehydrated subducted lithosphere (Hawkesworth et al., 1977). The low contents of Th and Ce in the three types as well as low La/Nb (1.6–1.7, 1.1 in A3), Th/Nb (0.04, 0.1 in A3), and Ta/Nb (0.05–0.06) rather exclude continental crust admixture to the magma source(s). The very low La/Yb and Th/Yb ratios may point to a primitive island arc setting (Condie, 1989), which is also in line with low Ce/Pb (~1.0 in A1 and A3) typical of arc basalts (Miller et al., 1994). The LILE enrichment relative to Nb and Ta may have been connected with dehydration of altered oceanic crust in a subduction zone (Saunders and Tarney, 1984). Summing up, the Rzeszotary amphibolite tholeiitic protoliths classify as intermediate between IAT and MORB, which is in line with the transitional setting of a back-arc basin (Pearce, 1996).

However, in view of the scarcity of the available rock material and very limited knowledge of the spatial relationships among the observed amphibolite types, interpretations of the origin and tectonic setting of the Mg- and Fe-tholeiitic precursors of the Rzeszotary amphibolites are not obvious. In A1 and A2, the flat REE pattern would suggest that the parent magma was not fractionated at the source, which might be consistent with the small negative to positive Eu anomaly ($Eu/Eu^* = 0.8–1.2$). The latter would indicate the lack of, or very minor, plagioclase accumulation. Lower contents of Ni, Cr, Mg and Yb (Appendix 1) in A1 than in A2 may possibly suggest greater depth of melting in the mantle in the case of A1, with melting probably triggered by decompression (Wilson, 1989; Cattel and Taylor, 1990). The CaO vs. MgO relationships (Herzberg and Asimow, 2008) and the FC3MS ($FeO/CaO-3*MgO/SiO_2$) parameters (Yang and Zhou, 2013) suggest that the protolith of A1 may have originated from partially melted peridotite whereas that of A2 was from pyroxenite.

In a few of the borehole cores, steep contacts between metagabbroic and metabasaltic variants are identifiable (Fig. 2), which may be however interpreted in two ways. Such contacts may have been either tectonic or intrusive (in the latter case, Fe-tholeiite (dykes?) would intrude the Mg-tholeiite domain).

FELSIC ROCKS

CLASSIFICATION

In the ~120 m long profile of borehole Rz 2 (Fig. 2), two types of gneiss, two types of granitoid and a leucocratic neosome in migmatitic amphibolites were analysed as felsic rocks. In the $K_2O + Na_2O$ vs. SiO_2 (wt.%) TAS diagram, the gneisses, migmatitic neosome and pinkish granite may be classified as granites, though they fall off the field of granite mainly due to high SiO_2 contents, whereas *Hbl*-granitoid classifies as granodiorite to diorite (Fig. 8L). All felsic rocks are acid, subalkaline, except for the K-granite which is alkaline. In the feldspar triangle (O'Connor, 1965; Barker, 1979), the *Pl*-*Ms*-gneiss falls within the field of tonalite, the *Ep*-gneiss and migmatitic neosome in the field of trondhjemite, while the pinkish K-granite and *Hbl*-granodiorite are in the field of granite (Fig. 8M). The two last have somewhat anomalously low Ca and Na contents. All the felsic rocks correspond to volcanic arc

granites (Fig. 8N), while the Ta/Yb vs. Th/Yb plot discriminates them between oceanic arc and active continental margin settings (Fig. 8O). In the Y+Nb vs. Rb diagram (Pearce, 1983), the K-granite is syn-collisional and the *Pl*-*Ms*-gneiss protolith straddles the VAG/syn-COLG border (Fig. 8P). The R1-R2 geotectonic diagram (Fig. 8R) classifies the K-granite as post-orogenic, and the *Hbl*-granodiorite and *Ep*-gneiss as syn-collisional rocks, while the migmatitic neosome and *Pl*-*Ms*-gneiss (metatonalite) are ascribed to mantle fractionates. However, despite some spread, all felsic samples fall in the area where the dividing lines meet, which affects the accuracy of the classification. These ambiguities may be also due to variable source chemistry or the later influence of metamorphic/migmatitic fluids.

In general, the Rzeszotary felsic rocks are quartz-rich with the La/Yb ratio ~30–60 and a Eu positive anomaly except for the *Hbl*-granodiorite (Appendix 1; Fig. 8S–U). In the classification of Frost et al. (2001), they are all magnesian, and either calcic (both gneisses and neosome) or alkali and alkali-calcic (K-granite and *Hbl*-granodiorite). On the Shand (1943) diagram, they are peraluminous except for the metaluminous neosome.

GENETIC CHARACTERISTICS AND IMPLICATIONS

The HREE contents are low in both *Ep*- and *Pl*-*Ms*-gneisses, still lower in the K-granite yet distinctly higher in the neosome in which they show almost equal abundances to primitive mantle. Ce is high (87–106 ppm) in the neosome ($Ce/Pb = 17.7$) and *Hbl*-granodiorite but low in the other felsic rocks ($Ce/Pb=0.5$ in Rz18 and 1.7 in *Ep*-gneiss). This concurs with the inferred mechanism of the neosome formation in migmatites, where initial metamorphic segregation was then extensively assisted by fluids presumably released from the developing and rising granitoid magma as well as by partial melting of gneisses (~700–620°C).

The K-granite and metatonalite have lower concentrations of HREE than the neosome and trondhjemite, yet the neosome is as rich in LREE as in the *Hbl*-*Ms* granodiorite, these elements being probably associated with fluid/melt mobility during the 2.0 Ga event. A positive Eu anomaly is characteristic of both the gneisses and K-granite, while the neosome and granodiorite do not display such an anomaly. This would be in line with their different evolution and/or contents of accessory minerals. All the felsic rocks have almost identical concentrations of Eu (Fig. 8S). In the K-granite, there are the lowest HREE and HFSE (Nb, Ta, Zr, Hf, U) contents but the highest abundances of Pb and LILE (K, Ba). The high lead content, most likely contained by K-feldspar, is consistent with the late/post-orogenic formation of the granite.

The felsic rocks in normalization to N-MORB and bulk continental crust, despite differences, generally display trace-element patterns characterized by enrichment in low field strength LIL elements (K, Rb, Cs, Ba, Pb, Sr, Eu) and some HFSE (Th, U, Zr, Hf) though by negative Nb, Ta and Ti anomalies and depletion in HREEs (Fig. 8S–U). In the case of the gneisses and neosome, these characteristics would suggest a suprasubduction setting, slab melting and slab-fluid release (Martin, 1999; Mohan et al., 2008; Adam et al., 2012) and, combined with a positive Sr anomaly, might imply an island arc or continental crust source. However, such characteristics may also indicate that in petrogenesis garnet, and not plagioclase, was a residual or fractionating phase (see Martin et al., 2005). Al_2O_3 contents (>12 wt.%), strongly fractionated REE ($(La/Yb)_N$ and $(La/Nb)_N$ ratios further suggest that garnet was in the residuum (Frost et al., 2001) which is in line with the positive Eu and

Sr anomalies usually attributed to plagioclase that crystallized from a felsic melt. Accordingly, high contents of incompatible Ba and Sr may be explained by partitioning into plagioclase and alkali feldspar. Thus, enrichment in Na relative to K in the Rzeszotary gneisses and neosome, when set against low La/Nb or Ta/Nb ratios but relatively high Ce/Pb, cannot be taken as indication of a continental geochemical signature.

Little/no plagioclase in the residue might signify that the high- Al_2O_3 protoliths of the gneisses originated due to differentiation of wet basaltic magma (in line with an Al_2SiO_5 phase in the *Ms-Pl*-gneiss) or by partial melting of basalts derived from such magma (Barker and Arth, 1976). Another option of their origin would be partial melting of amphibolites (*Hbl-Pl* \pm *Qtz* \pm *Grt*) that left behind a *Prx-Grt*-rich residue (Moyen and Martin, 2012). Whatever origin of the peraluminous gneiss protoliths, they seemed to form in temperatures $>740^\circ\text{C}$ as indicated by the zircon-saturation (Harrison and Watson, 1983) and apatite-saturation with ASI-correction (Bea et al., 1992), which amount to $765\text{--}788^\circ\text{C}$ in the case of tonalite and to $822\text{--}878^\circ\text{C}$ in trondhjemite. The estimates conform to those based on $\text{Al}_2\text{O}_3/\text{TiO}_2$ ratios (Jung and Pfander, 2007) which, calculated with the GCDKit software (Janoušek et al., 2006) for amphibolite melting, gave 740°C (tonalite) and 850°C values (trondhjemite), respectively. Such estimates made for the K-granite yielded similar values of $790\text{--}835^\circ\text{C}$ (accessory mineral saturation) and of 735°C ($\text{Al}_2\text{O}_3/\text{TiO}_2$ thermometry). The scatter of the results may have been caused by disequilibrium partial melting of the arc lower crust.

In the Rzeszotary Terrane, the *Hbl*-granodiorite significantly differs from the other felsic rocks by having moderate SiO_2 (~ 63 wt.%), the highest concentration of REE, and relatively high contents of Al_2O_3 , Fe_2O_3 , MgO as well as Cs, Nb, Ta, Th, U, Gd, La, Yb, V (Th and La are yet higher in the neosome; Fig. 8S–U). Such features locate the granodiorite between the mafic and felsic rocks (Fig. 8A, B, L). The borehole core sampled in fact includes brecciated amphibolite lumps (Fig. 5H), thus the injecting granitoid magma may be contaminated by the mafic country rock and the sample may not be representative.

Sm-Nd ISOTOPES

Four samples were subjected to whole-rock Sm-Nd isotopic analysis: A1 and A2 amphibolites, migmatitic neosome and K-granite. For both felsic rocks, zircon U-Pb ages were determined by SHRIMP. Granite intrusion and migmatization took place at 2.0 Ga, whereas the inherited zircons in the neosome indicated either a protolith age of the mafic mesosome or an early stage of metamorphism of the gabbroic protolith at 2.75–2.6 Ga (Żelaźniewicz and Fanning, 2020).

All rocks analysed revealed negative $\text{Nd}(0)$. The two amphibolite samples have high Sm/Nd ratios (Appendix 3), which would put in doubt calculation of model ages (Stern, 2002). By contrast, both neosome and K-granite have relatively low Sm/Nd and yielded T_{DM} ages of 3.04 and 2.8 Ga, respectively, according to the one-stage linear model of Goldstein et al. (1984) and Goldstein (1988). These indicate that protoliths of the two felsic rocks separated from the mantle in Meso- and Neoproterozoic times. In general, negative $\text{Nd}(2000)$ values suggest that all the Rzeszotary rocks come from source(s) enriched in LIL and not from the depleted part of the reservoir(s). Different Nd initial ratios are in line with derivation from different source regions. In the metabasites A1 and A2, similar enrichment factors $f^{\text{Sm/Nd}}$ (DePaolo and Wasserburg, 1976) of -0.1 and -0.2 , respectively, indicate that fractionation of Sm and Nd did not vary significantly in the time interval in which the two were formed, yet the rocks seem not cogenetic.

The neosome (Rz17) of $T_{\text{DM}}(\text{Nd})$ age of ~ 3.0 Ga developed in the amphibolite (A1–A3) which was migmatized mainly by the segregation mechanism. Such an origin implies that the protolith of the metabasite may have had a similar model age (though an older one cannot be excluded). This would agree with the scenario proposed of an inferred oceanic arc, which suggests that the tholeiitic protolith of the A1 metagabbro must have been separated from the mantle earlier in the Archean and that gabbroic additions (original protolith of neosome Rz17) to the arc crust may probably have continued at least to 3.0 Ga. Out of the four samples analysed, the A1 metagabbro displays the relatively highest $\text{Nd}(T)$ values of -0.08 at 2.0 Ga or $+1.53$ at 2.65 Ga, which indicates the most juvenile components in its protolith. This is in line with the relatively least evolved chemical composition of amphibolite A1. In case of neosome Rz17, being the ultimate product of transformation (= migmatization) of the metamorphic rock whose protolith came from the initial arc gabbro, the negative $\text{Nd}(T)$ values of -13.7 Ga at 2.0 Ga and -2.8 at 2.65 Ga may have reflected enrichment gained during ongoing Neoproterozoic–Paleoproterozoic subduction, though more likely the contamination was brought about by alkali fluid-assisted migmatization at 2.0 Ga.

Less obvious are the negative $\text{Nd}(T)$ values of -6.73 Ga at 2.0 Ga and of -3.26 at 2.65 Ga for amphibolite A2 as such negative signatures are rather anomalous for mantle-derived basalts. The A2 protolith was subalkaline, Fe-tholeiitic basalt which was significantly more evolved than A1, which concurs with the comparatively lower $\text{Nd}(T)$ and subduction-related LILE enrichment (Appendix 1). Although the two do not differ in their LREE abundances (Fig. 8J, K), A2 is richer in LILE and has slightly higher contents of HREE. The geochemical characteristics do not favour fractionation, thus such differences may point to mantle heterogeneity or indicate different parent reservoirs (DePaolo and Wasserburg, 1976). The small number of available samples do not allow solution of this question, which leaves room for further speculation.

The $T_{\text{DM}}(\text{Nd})$ age of 2.8 Ga for K-granite is the youngest among the Rzeszotary rocks analysed, which in a way is consistent with its intrusion at 2.0 Ga as the youngest lithological element in the Rzeszotary complex (Żelaźniewicz and Fanning, 2020). Such a position is also reflected by highly negative $\text{Nd}(0)$ values, as low as -8.8 at the time of intrusion. In view of untypically low Na contents (and very high Ba), the provenance of the K-granite magma may have been linked with melting of the predominant tonalitic components of the Rzeszotary complex (*Ms-Pl*-gneisses) that were earlier built into the original arc crust. If so, the TDM age of 2.8 Ga may have indicated the time when a mafic precursor of the Na-tonalite was formed in the then still developing arc edifice. Nevertheless, other protolith(s) cannot be excluded as suggested by the presence of Mg-rich garnet, which does not occur in any other rock member of the complex. Therefore, one can speculate about “exotic” sources, for instance a partially melted felsic granulite. Such a suspect granulite may have come from the colliding cratonic crust of the $T_{\text{DM}}(\text{Nd})$ age of 2.8 Ga.

DISCUSSION

A positive correlation of generally immobile HFSE (Nb, Hf, La) against Zr suggests that abundances of these elements were not significantly disturbed during metamorphism (e.g., Winchester and Floyd, 1977; Pearce and Norry, 1979; Wilson, 1989) and deformation of the Rzeszotary rocks, thus their geochemical characteristics may be utilized for some genetic con-

siderations (Fig. 8E, G, I), even though the rock systems might not have been entirely closed.

GEOCHEMICAL CONSTRAINTS ON PROTOLITH CHARACTER

Protoliths of the Rzeszotary amphibolites presumably originated by partial melting of primary mantle peridotite, which eventually gave rise to basaltic rocks (Barker, 1979). The process of segregation from the primitive mantle likely took place at a depth below plagioclase “stability” where metastable garnet was in the residue (Martin et al., 2005). This may have occurred at the base of the inferred arc/back-arc. The La/Sm ratios of 2.06–3.16 and La/Nb ratios of 1.7–1.6 (1.1 in A3) along with the Nb/La ratio <1 are compatible with an oceanic arc and subduction setting (Cook et al., 2016). A subduction component might be also suggested from some trace element relationships as for instance the Nb/Yb vs. Th/Yb diagram (Pearce, 2008) in which the spread of A1–A2 points seems to follow the subduction component vector.

Summarizing, the scenario proposed assumes that the HREE-depleted Rzeszotary tholeiite source(s) was in the juvenile upper mantle without admixtures from continental crust but with some additions from subducted oceanic lithosphere and possibly metasomatised mantle. They were eventually emplaced in the extensional regime of an arc/back-arc setting in an overall convergent environment.

The Rzeszotary gneisses and migmatitic neosome display high contents of SiO₂ (>72 wt.%) and Al₂O₃ (11.5–15.25 wt.%), low contents of ferromagnesian elements (Fe₂O₃+MgO+ MnO+ TiO₂ <2.5 wt.%), low HREE ratios (Appendix 1) and low the (La/Yb)_N vs Yb_N ratios. Such characteristics, combined with low Nb, Ta, Ti contents and positive Sr–Pb anomalies, are akin to the tonalite-trondhjemite associations that are common in Archean–Paleoproterozoic terrains (Fig. 8I–K). The small number of samples inhibits general comparisons yet similarities to the TTG series seem evident (Moyen and Martin, 2012).

The gneisses underwent metamorphism and migmatization, thus together with the neosome are older than the unfoliated K-granite and *Hbl*-granodiorite, being late- to post-metamorphic/post-tectonic intrusive rocks. The two groups with Mg# < 45 differ in contents of Na₂O (~4–6% vs. 1.3–2%), K₂O (1.1–1.6% vs. 4.5–8.2%) and CaO (1.3–3.6% vs. 0.3–0). The peraluminous gneisses, with K₂O < 3 wt.%, Na₂O/K₂O > 1.5 and I-type signature, probably did not originate from the partially melted felsic crust. In the case of the neosome, the metaluminous composition supports the segregation mechanism inferred for the migmatization of the A1 amphibolites. Unusually high contents of Ni and Cr, similar to those in the amphibolites (A1 in particular), point to the original connection of the gneiss protoliths with the parent arc mantle. A precursor of the *Pl*-*Ms*-gneisses (~tonalites) may have formed by partial melting of MORB/enriched tholeiitic basalt source at the base of an island arc at temperatures of ~765–790°C. Water needed to promote such process might have been supplied by hydrous magmas generated within the subduction zone. In the case of the *Ep*-gneisses (~trondhjemite), partial melting of both tonalitic crust and mafic rocks/basaltic amphibolites at temperatures of 820–880°C may be suggested (Wolf and Wylie, 1994; Moyen and Martin, 2012), or melting of garnet-amphibolite represented by the *Grt*-in residue (without plagioclase) after tonalite melt had been segregated from the basaltic source, which however seems a less probable alternative.

Characteristically, the *Ep*-gneisses appear only within the amphibolites (Fig. 2). As compared to the *Pl*-*Ms*-gneisses (tonalites), they are richer in Si but poorer in Al and some LIL elements (K, Ba) (Appendix 1). On the other hand, a few amphi-

bolite fragments up to several centimetres thick set in the *Pl*-*Ms*-gneisses may be considered mafic xenoliths entrapped in original tonalites on emplacement, or alternatively as later mafic veins that intruded the tonalites.

In general, peraluminous granite/melt may be formed by water-excess melting of mafic rocks or metaluminous felsic rocks. The composition of the 2.0 Ga pinkish K-granite (low Na and Ca, high Ba and Rb) is a little ambiguous, especially in view of the presence of relic pyrope-almandine garnet, whose remnants may have been possibly inherited from an older HP domain (granulites?) of unknown age and provenance. An estimated temperature of ~800°C (Zr-saturation thermometer), large positive Eu anomaly with respect to low Sm and Gd (Fig. 8S, T) and very low HREE abundances resemble a leucosome melt, thus infracrustal melting of earlier felsic rocks (= *Pl*-*Msg*-gneisses) rather than melting of amphibolites. The earlier-formed dominantly metatonalitic Rzeszotary crust might have been a suitable source (Żelaźniewicz and Fanning, 2020). Subduction would then provide enough water to allow and promote vapor-present partial melting of the felsic crustal component as well as hydrous metamorphism with K-metasomatism and migmatization conspicuous in the metabasic elements of the crust.

TECTONOMETAMORPHIC EVOLUTION

Legible mineral records (classical geothermobarometers and thermodynamic modeling) show that igneous protoliths of the Rzeszotary complex underwent metamorphic transformations within a *P*-*T* range of 500–700°C/6–12 kbar, with the peak temperature exceeding 650°C. Mafic rocks were metamorphosed to *Hbl*-*Alm*-*Grs*-*Grt*-*Ep*-amphibolite while tonalite and trondhjemite (TTs) were transformed to *Pl*-*Ms*-gneisses and *Ep*-gneisses, respectively. Epidote developed at the expense of originally more Ca-rich plagioclase. In the amphibolites, Ca-garnet coexists with albitic plagioclase, which may suggest that Ca was partitioned into garnet. These processes took place at ~2.0 Ga (Żelaźniewicz and Fanning, 2020).

The results of thermodynamic modeling, generally consistent with classic thermobarometric calculations and in line with the compositional zonation in the minerals, also documented the (post?)peak and retrograde part of a clockwise *P*-*T* path. Exhumation and retrogression occurred at temperatures dropping to close to 450°C and pressures around 8–4 kbar, thus at greenschist facies conditions. The latter were associated with ductile/brittle shearing and accompanied by localized chloritization of amphiboles and garnets, which must have taken place after the ~2.0 Ga event but before deposition of the lower Cambrian cover (Żelaźniewicz and Fanning, 2020). It seems most likely that the Rzeszotary complex underwent a Neoproterozoic overprint because of involvement in the Cadomian Orogen as part of its foreland basement (Żelaźniewicz et al., 2009, 2020).

An early HP event hinted by observations in both felsic and mafic rocks is disputable. The suspect relict of a feasible HP assemblage (Al₂SiO₅; relict kyanite, andalusite?) found in the *Pl*-*Ms*-gneiss may be likely explained as an Al-phase that crystallized when feldspars and white mica in the peraluminous granite precursor of the very gneiss could not accommodate any more aluminum (Frost et al., 2001). The single sample of amphibolite A2 that carries suspect HP fragments (sadanagaite?) also locally contains actinolite. The latter irregularly replaces Mg-hornblende in its inside, at its margins and along cleavage/cracks. Next to such actinolite rims, K-feldspar appears (Fig. 6H) and Al-rich titanite is present. These occurrences suggest retrograde hydration processes and the influ-

ence of alkali fluids. Conditionally applied geothermobarometers approximate P - T conditions of 5.8–2.7 kbar/400–340°C. The lowest values were obtained for the actinolite in the cracks. In conjunction with the chloritization seen in amphibole and garnet grains, such observations point to a greenschist overprint, also indicated by the thermodynamic modeling noted above.

In contrast, yet another suspect trace of an earlier higher pressure episode in the evolution of the Rzeszotary complex is rendered by a few Mg-rich but Ca-poor garnet relicts preserved in the 2.0 Ga K-granite. Such relicts apparently survived partial melting of crustal rocks which produced the granite. Their composition suggests inheritance from an older HP felsic granulite protolith.

The data collected show that synmetamorphic migmatization brought about segregation of minerals into neosome and mesosome with slightly altered palaeosome, which was accomplished by metamorphic differentiation assisted by fluids, partial melting and leucocratic magmatic/migmatitic neosome injections (Fig. 3E). Alkali-carrying aqueous fluid infiltrations were presumably connected with the formation of K-rich granitoid magma deeper in the crust, which was likely a source for the 2.0 Ga K-granite intrusions/injections into metamorphic rocks of the Rzeszotary complex.

In the migmatized Pl - Ms -gneisses, plagioclase grains locally display like-like boundaries, which is characteristic of migmatitic differentiation (Ashworth and McLellan, 1985). This process was assisted by inter- and intragranular infiltrations of alkali fluids and operated along with vapor-present partial melting. Such a complex interplay of mechanisms did not require very high temperatures to eventually bring about migmatization of the Rzeszotary felsic rocks. However, the calculated temperatures were apparently too low to cause melting in the amphibolites. Therefore, the mafic rocks were migmatized mainly by metamorphic segregations enhanced by volatiles and by injections of Ab - Kfs - Oz melts that originated in the felsic domains.

The presence of magmatic melt is inferred from the presence of quartz rims around K-feldspar phenocrysts and of large rounded quartz grains with K-feldspar–quartz coronitic texture as indicative of reaction processes between the phenocrysts and melt, and from embayments in the plagioclase that indicate corrosion during melt solidification (e.g., Vernon, 2011). Moreover, in the migmatized amphibolites and amphibole gneisses, the rheological contrast between plagioclase on one hand and K-feldspar and quartz grains on the other suggests that the two latter crystallized later and were linked with the mobile phase which contributed to the increasing pore-pressure that eventually resulted in semi-brittle deformation of plagioclase. Amphibolite lumps set in the granodioritic matter in the fault zone (Fig. 6D) suggest a hydraulic fracturing mechanism when the granite was forced up to higher/shallower levels in the crust.

Structural observations show that synmetamorphic tectonic deformation under amphibolite facies conditions was accomplished in a contractional regime, with strain intensified in the shear zones (Fig. 5). Mineral lineations and kinematic criteria point to mainly dip-slip movements with evidence of earlier thrusting up-dip and later normal down-dip shearing (Fig. 5F; Żelaźniewicz and Fanning, 2020: fig. 5). A tectonic event accompanied by thrusting undoubtedly took place prior to the 2.0 Ga granite intrusion. However, the subsequent normal overprint remains unconstrained, yet must have happened before concealment under the lower Cambrian platform deposits, thus may have been Cadomian at the latest.

Considering the presence of several shear zones (Fig. 2) in the migmatized amphibolite portion of the interval drilled, it cannot be excluded, nor demonstrated, that the upper, mainly

gneissic domain and the lower, mainly metabasitic domain were structurally juxtaposed by thrust shearing. In any event, tectonic contacts between rheologically different members of the Rzeszotary complex can be expected.

The K-granite penetrated the country rocks both as sills and dykes along fracture zones. Injections of the pinkish granite, which presumably originated by partial melting of earlier metamorphosed crustal rocks, terminated the tectonothermal event in the Rzeszotary complex ~2.0 Ga (Żelaźniewicz and Fanning, 2020).

PROVENANCE IMPLICATIONS

On the Rzeszotary Horst, two discrete events were revealed by U-Pb zircon dating at ~2.7–2.6 Ga and 2.0 Ga (Żelaźniewicz and Fanning, 2020). The earlier event was presumably related to an intraoceanic arc and back-arc extension. It produced juvenile crust, parts of which were at ~2.0 Ga eventually accreted by continental margin subduction to one of the then cratons. This might have been North and South America, West Australia, Africa, China or East Europe as they were all involved in orogenic processes connected with the formation of a Paleoproterozoic supercontinent (Condie and Kröner, 2013; Condie, 2016). The Rzeszotary basement was likely formed by those global processes though the parent continent is difficult to identify unambiguously (Żelaźniewicz and Fanning, 2020).

Tectonothermal evolution of the Rzeszotary gneisses and amphibolites terminated with the intrusion of the 2.0 Ga post-tectonic K-granite derived from melting of older crust at temperatures of 735–835°C. This assemblage may be considered as part of a larger continental entirety to which a Neoproterozoic (~2.7–2.6 Ga) juvenile arc was accreted at ~2.0 Ga to form part of the then global orogenic edifice (Zhao et al., 2002, 2011). Searching for the cradle of the Rzeszotary complex strongly depends on the available knowledge concerning the geological evolution of the potential suspect parent terrains. Various details of this complex, given in this and a companion paper (Żelaźniewicz and Fanning, 2020), have been provided with the intention to help such further correlations. The 2.0 Ga events may be part of the 2.1–1.8 Ga narrative of assembling of the then continental masses into the supercontinent of Columbia (Zhao et al., 2002, 2011), with the Rzeszotary basement likely being a part of this. In the Rzeszotary Terrane, the 2.0 Ga granitic magma was formed at the end of a collisional orogenic event. A suspect granulite component may have come from the colliding craton. The $T_{DM}(Nd)$ age of 2.8 Ga would then relate to the cratonic crust.

In the Brunovistulia superterrane, the Rzeszotary Horst represents its easternmost and evidently the oldest, Neoproterozoic–Paleoproterozoic, component that formed (part of the) basement to the Cadomian foreland in the Upper Silesian part of this orogenic belt (Żelaźniewicz et al., 2009). The Rzeszotary Terrane became involved in the Cadomian belt during the Tonian–Ediacaran re-assembly of continental fragments that resulted from the break-up of Rodinia (Nawrocki et al., 2004; Żelaźniewicz et al., 2009, 2020). The Cadomian foreland succession is known from the northern and eastern Upper Silesia Block (Fig. 1). It was folded and anchimetamorphosed with the formation of a conspicuous cleavage oblique to well-preserved bedding (Żelaźniewicz et al., 2009). The Rzeszotary basement was not involved in the foreland deformation, probably except through faulting and jointing, though it may have been affected by a very low-grade overprint observed as chloritization of garnet and amphibole in the gneisses and amphibolites. The Rzeszotary horst, in which the Cadomian foreland basement was encountered by drilling is part of the Upper Silesia Block

whose central and western fragments underwent intensive arc magmatism between 620–540 Ma and represent the Cadomian internides. As the Cadomian hinterland and foreland basement differ dramatically, the Rzeszotary complex is interpreted as the Rzeszotary Terrane, one more constituent of the Brunovistulia superterrane (Kalvoda, 2008; Żelaźniewicz et al., 2009, 2020; Kalvoda and Bábek, 2010). Consequently, the Rzeszotary Terrane has to be considered as an important component of the Cadomian orogenic belt and taken into account in reconstructions of the evolution and geotectonic position of Brunovistulia.

SUMMARY AND CONCLUSIONS

Closer characterization of the Rzeszotary rocks combined with the data presented in the earlier companion paper (Żelaźniewicz and Fanning, 2020) shed more light on the composition, provenance and evolution of the Precambrian basement penetrated by the Rz 2 borehole, in the Upper Silesia Block of the Brunovistulia superterrane, which may be tentatively highlighted as follows below.

Prior to or around 3.2–3.0 Ga, precursors of the Rzeszotary complex were separated from depleted mantle and contributed to oceanic lithosphere. At 2.75–2.6 Ga, oceanic subduction led to the formation of a juvenile magmatic arc edifice (Nd(T) of +1.53). Back-arc extension promoted upwelling and decompression melting of the depleted mantle, which brought about tholeiite magmas of IAT/MORB composition with LILE additions owing to the fluids released from the subducting slab. Such magma underplated the arc and contributed as a gabbroic/basaltic (negative Nd) component to its lower crust. Tonalite was formed at that time due to partial melting of the mantle-derived wet basalts (~740°C) at the base of the island arc. During ongoing upwelling and decompression, mantle also melted at shallower depths, which resulted in HFSE-enriched Fe-tholeiite magma, more abundant in HREE. A trondhjemitic precursor of *Ep*-gneisses, that penetrated and intruded the tholeiites, may have originated by partial melting (~850°C) of metamorphosed wet basalts of the subducted slab.

Around 2.0 Ga, the arc collided with an unspecified cratonic mass and yielded to orogenic deformation, metamorphism and migmatization. The entire arc edifice was then strongly shortened and the earlier back-arc crust/mantle products were

forced down to ~6–12 kbar depths where they underwent contractional deformation and metamorphism (700–500°C) that overprinted and strongly obliterated older effects of a 2.75–2.6 Ga event. The tonalites and trondhjemitites were metamorphosed to *Pl*-*Ms*-gneisses and *Ep*-gneisses, and the gabbros and basalts to epidote-amphibolites and garnet-amphibolites. Synmetamorphic shortening of the rock pile led to folding documented by variations in the foliation attitude and heterogeneous development of shear zones with thrust kinematics.

The amphibolite facies metamorphism graded to migmatization, conspicuous in the metabasites, and the process of segregation/differentiation was assisted by fluid penetration, facilitated by the shear-promoted channels, and by partial melting. This event was terminated by intrusions of alkaline peraluminous magma that solidified to K-granites (Nd(T) of –9) at 2.0 Ga and minor *Hbl*-granodiorite (undated). Granite intrusions were in some places accompanied by hydraulic fracturing and syn-intrusive brecciation during normal faulting. The phengitic mica K-granite retained some Mg-rich garnet relicts, probably indicative of older HP rocks (granulites?), at the expense of which it developed at temperatures of >735°C.

These metamorphic-migmatitic phenomena seem to have occurred almost coevally at ~2.0 Ga, presumably in direct connection with the 2.1–1.8 Ga global event and the amalgamation of the Paleoproterozoic supercontinent of Columbia. We suggest that the Neorchean–Paleoproterozoic rocks drilled by the Rz 2 borehole represent a small part of a large orogenic edifice assembled within Columbia. A fragment of that edifice, now the Rzeszotary Terrane, was then detached from the mainland, re-assembled and eventually in the Neoproterozoic became part of the foreland of the Cadomian Orogen in Central Europe, specifically a part of the composite terrane of Brunovistulia (Żelaźniewicz et al., 2020).

Acknowledgements. Financial support for this work was available through project 2017/25/B/ST10/02927 (National Science Centre, Poland) and partly from project PCZ-07-21 (Ministry of Environment, State Committee for Scientific Research, Poland), which is gratefully acknowledged. A. Muszyński and T. Oberc-Dziedzic are thanked for critically reading and discussing an earlier version of the paper. Two anonymous reviewers are thanked for their helpful and inquisitive comments.

REFERENCES

- Adam, J., Rushmer, T., O'Neil, J., Francis, D., 2012. Hadean greenstones from the Nuvvuagittuq fold belt and the origin of the Earth's early continental crust. *Geology*, **40**: 363–366.
- Ashworth, J.R. (ed.), 1985. *Migmatites*. Blackie & Son.
- Ashworth, J.R., McLellan, M.C., 1985. Textures. In: *Migmatites* (ed. J.R. Ashworth): 180–203. Blackie & Son.
- Barker, F., 1979. Trondhjemitite: definition, environment and hypotheses of origin. *Developments in Petrology*, **6**: 1–11.
- Barker, F., Arth, J.G., 1976. Generation of trondhjemitic-tonalitic liquids and Archean bimodal trondhjemitite-basalt suites. *Geology*, **4**: 596–600.
- Batchelor, R.A., Bowden, P., 1985. Petrogenetic interpretation of granitoid rock series using multicationic parameters. *Chemical Geology*, **48**: 43–55.
- Bea, F., Fersther, G., Corretgé, L.G., 1992. The geochemistry of phosphorus in granite rocks and the effect of aluminium. *Lithos*, **29**: 43–56.
- Blundy, J.D., Holland, T.J.B., 1990. Calcic amphibole equilibria and a new amphibole-plagioclase geothermometer. *Contributions to Mineralogy and Petrology*, **104**: 208–224.
- Buła, Z., 2000. Lower Paleozoic of Upper Silesia and West Małopolska. (in Polish with English summary). *Prace Państwowego Instytutu Geologicznego*, **171**: 1–63.
- Burtan, J., 1962. Borehole Rzeszotary 2 (in Polish with English summary). *Kwartalnik Geologiczny*, **6** (2): 245–259.
- Cattell, A.C., Taylor, R.N. 1990. Archean basic magmas. In: *Early Precambrian basic magmatism* (eds. R.P. Hall and D.J. Hughes): 36–37. Glasgow and London, Blackie.

- Cieśla, E., Wybraniec, S., Petecki, Z., 1993.** Mapa magnetyczna Polski w skali 1:200 000 z komputerowym bankiem danych (in Polish). Centr. Arch. Geol. Państwowy Instytut Geologiczny, Warszawa.
- Condie, K., 1989.** Plate Tectonics and Crustal Evolution. Pergamon Press, Oxford.
- Cook, Y.A., Sanislav, I.V., Hammerli, J., Blenkinsop, T.G., Dirks, P.H.G.M., 2016.** A primitive mantle source for the Neoproterozoic mafic rocks from the Tanzania Craton. *Geoscience Frontiers*, **7**: 911–9260.
- Cox, K.G., Bell, J.D., Pankhurst, R.J., 1979.** The Interpretation of Igneous Rocks. Allen and Unwin, London.
- DePaolo, D.J., Wasserburg, G.J., 1976.** Nd isotopic variations and petrogenetic models. *Geophysical Research Letters*, **3**: 249–252.
- Dudás, F.O., 1992.** Petrogenetic evolution of trace element discrimination diagrams. *Basement Tectonics*, **8**: 93–127.
- Dudek, A., 1980.** The crystalline basement block of the Outer Carpathians in Moravia: Bruno-Vistulicum. *Rozprawy České Akademie Věd, Řada mathematicko-přírodovědeckých Věd*, **90**: 1–85.
- Finger, F., Frasl, G., Dudek, A., Jelínek, E., Thöni, M., 1995.** Cadomian plutonism in the Moravosilesian basement. In: *Tectonostratigraphic Evolution of the Central and East European Orogens* (eds. R.D. Dallmeyer, W. Franke and K. Weber): 495–507. Springer, Heidelberg.
- Finger, F., Hanžl, P., Pin, C., Von Quadt, A., Steyrer, H.P., 2000.** The Brunovistulian: Avalonian Precambrian sequence at the eastern and of the Central European Variscides? *Geological Society Special Publications*, **179**: 103–112.
- Friedl, G., Finger, F., McNaughton, N.J., Fletcher, I.R., 2000.** Deducing the ancestry of terranes: SHRIMP evidence for South America-derived Gondwana fragments in central Europe. *Geology*, **28**: 1035–1038.
- Frost, R.B., Barnes, C.G., Collins, W.J., Arculus, R.J., Ellis, D.J., Frost, C.D., 2001.** A geochemical classification of granitic rocks. *Journal of Petrology*, **42**: 2033–2048.
- Goldstein, S.L., 1988.** Decoupled evolution of Nd and Sr isotopes in the continental crust. *Nature*, **336**: 73–738.
- Goldstein, S.L., O’Nions, R.K., Hamilton, P.J., 1984.** A Sm-Nd study of atmospheric dusts and particulates from major river systems. *Earth and Planetary Science Letters*, **70**: 221–236.
- Gribble, R.F., Stern, R.J., Bloomer, S., Stuben, D., Ohearn, T., Newman, S., 1996.** MORB mantle and subduction components interact to generate basalts in the southern Mariana through back-arc basin. *Geochimica et Cosmochimica Acta*, **60**: 2153–2166.
- Hammarstrom, J.M., Zen, E-an, 1986.** Aluminum in hornblende: an empirical igneous geobarometer. *American Mineralogist*, **71**: 1297–1313.
- Harrison, T.M., Watson, E.B., 1983.** Kinetics of zircon dissolution and zirconium diffusion in granitic melts of variable water content. *Contributions to Mineralogy and Petrology*, **84**: 66–72.
- Hawkesworth, C.J., O’Nions, R.K., Pankhurst, R.J., Hamilton, P.J., Evensen, N.M., 1997.** A geochemical study of island-arc and back-arc tholeiites from the Scotia sea. *Earth Planetary Letters*, **36**: 253–262.
- Hawthorne, F.C., Oberti, R., Harlow, G.E., Maresch, W.V., Martin, R.F., Schumacher, J.C., Welch, M.D., 2012.** Nomenclature of amphibole supergroup. *American Mineralogist*, **97**: 20131–2048.
- Haydutow, I., Yanev, S., 1995.** The Protomoesian microcontinent of the Balkan Peninsula – a peri-Gondwanaland piece. *Tectonophysics*, **272**: 303–313.
- Heflik, W., Konior, K., 1974.** The present state of knowledge concerning the crystalline basement in the Cieszyn-Rzeszotary area (in Polish with English summary). *Biuletyn Instytutu Geologicznego*, **273**: 195–221.
- Herzberg, C., Asimow, P.D., 2008.** Petrology of some oceanic island basalts: PRI-MELT2. XLS software for primary magma calculation. *Geochemistry, Geophysics, Geosystems*, **9**: 1–25.
- Holland, T., Blundy, J., 1994.** Non-ideal interactions in calcic amphiboles and their bearing on amphibole-plagioclase thermometry. *Contribution to Mineralogy and Petrology*, **116**: 433–447.
- Holland, T.J.B., Powell, R., 1998.** An internally consistent thermodynamic data set for phases of petrological interest. *Journal of Metamorphic Geology*, **16**: 309–343.
- Irvine, T.N., Baragar, W.R.A., 1971.** A guide to the chemical classification of the common volcanic rocks. *Canadian Journal of Earth Sciences*, **8**: 523–548.
- Janoušek, V., Farrow, C.M., Erban, V., 2006.** Interpretation of whole-rock geochemical data in igneous geochemistry: introducing Geochemical Data Toolkit (GCDkit). *Journal of Petrology*, **47**: 1255–1259; GCDkit 3.0 v. 2013.
- Jastrzębski, M., Żelaźniewicz, A., Sláma, J., Machowiak, K., Śliwiński, M., Budzyń, B., Jaźwa, A., Kocjan, I., 2021.** Provenance of Precambrian basement of the Brunovistulian Terrane: new data from its Silesian part (Czech Republic, Poland), central Europe, and implications for Gondwana break-up. *Precambrian Research*, doi.org/10.1016/j.precamres.2021.106108
- Jensen, L.S., 1976.** A new cation plot for classifying subalkalic volcanic rocks. *Ontario Division of Mines Miscellaneous Paper*, **62**: 1–22.
- Jung, S., Pfänder, J.A., 2007.** Source composition and melting temperatures of orogenic granitoids – constraints from CaO/Na₂O, Al₂O₃/TiO₂ and accessory mineral saturation thermometry. *European Journal of Mineralogy*, **19**: 859–870.
- Kalvoda, J., Bábek, O., 2010.** The margins of Laurussia in central and southeast Europe and southwest Asia. *Gondwana Research*, **17**: 526–545.
- Kalvoda, J., Leichmann, J., Bábek, O., Melichar, R., 2003.** Brunovistulian terrane (Central Europe) and Istanbul Zone (NW Turkey): Late Proterozoic and Paleozoic tectonostratigraphic development and paleogeography. *Geologica Carpathica*, **54**: 139–152.
- Kalvoda, J., Bábek, O., Fatka, O., Leichmann, J., Melichar, R., Nehyba, S., Spacek, P., 2008.** Brunovistulian terrane (Bohemian Massif, Central Europe) from late Proterozoic to late Paleozoic: a review. *International Journal of Earth Sciences*, **97**: 497–518.
- Konior, K., 1974.** Geological structure of the Rzeszotary elevation in the light of recent geophysical and drilling data (in Polish with English summary). *Annales Societatis Geologorum Poloniae*, **44**: 321–375.
- Królikowski C., Petecki, Z., 1995.** Gravimetric Atlas of Poland. Państwowy Instytut Geologiczny, Warszawa.
- Leake, B., Woolley, A.R., William, C.E.S., Birch, D., Gilbert, M.C., Grice, J.D., Hawthorne, F.C., Hanan, J., Kisch, H.J., Krivovichev, V.G., Linthout, K., Mandarino, J.A., Maresch, W.V., Nickel, E.H., Rock, N.M.S., Schumacher, J.C., Smith, D.C., Stephenson, N.C.N., Ungaretti, L., Whittaker, E.J.W., Youzhi, G., 1997.** Nomenclature of amphiboles; Report of the Subcommittee on Amphiboles of the International Mineralogical Association, Commission on New Minerals and Mineral Names. *The Canadian Mineralogist*, **35**: 219–246.
- Martin, H., 1999.** Adakitic magmas: modern analogues of Archean granitoids. *Lithos*, **46**: 411–429.
- Martin, H., Smithies, R.H., Rapp, R.P., Moyen, J.-F., Champion, D.C., 2005.** An overview of adakite, tonalite–trondhjemite–granodiorite (TTG) and sanukitoid: relationships and some implications for crustal evolution. *Lithos*, **79**: 1–24.
- Mehnert, K.R., 1968.** Migmatites and the Origin of Granitic Rocks. Elsevier, Amsterdam, New York.
- Miller, D.M., Goldstein, S.L., Langmuir, C.H., 1994.** Cerium/lead and lead isotope ratios in arc magmas and the enrichment of lead in the continents. *Nature*, **368**: 514–520.
- Mohan, M.R., Kamber, B.S., Piercey, S.J., 2008.** Boron and arsenic in highly evolved Archean felsic rocks: implications for Archean subduction processes. *Earth and Planetary Science Letters*, **274**: 479–488.
- Moyen, J.-F., Martin, H., 2012.** Forty years of TTG research. *Lithos*, **148**: 312–336.

- Mullen, E.D., 1983.** MnO/TiOz/ PzOs: a minor element discriminant for basaltic rocks of oceanic environments and its implications for petrogenesis. *Earth Planetary Science Letters*, **62**: 5–62.
- Nakamura, N., 1974.** Determination of REE, Ba, Fe, Mg, Na and K in carbonaceous and ordinary chondrites. *Cochim. Cosmochim. Acta*, **38**: 757–775.
- Nawrocki, J., Żylińska, A., Buła, Z., Grabowski, J., Krzywiac, P., Poprawa, P., 2004.** Early Cambrian location and affinities of the Brunovistulian terrane (Central Europe) in the light of palaeomagnetic data. *Journal of the Geological Society*, **161**: 513–522.
- Nowak, J., 1927.** Zarys geologii Polski (in Polish). II Zjazd Stowarzyszenia Geologów i Etnografów. Kraków.
- Oberc-Dziedzic, T., Kryza, R., Klimas, K., Fanning, M.C., 2003.** SHRIMP U/Pb zircon geochronology of the Strzelin gneiss, SW Poland: evidence for a Neoproterozoic thermal event in the Fore-Sudetic Block, Central European Variscides. *International Journal of Earth Sciences*, **92**: 701–711.
- O'Connor, J.T., 1965.** A classification for quartz-rich igneous rocks based on feldspar ratios. U.S. Geological Survey Professional Paper, **525**: 79–84.
- Pearce, J.A., 1983.** Role of the sub-continental lithosphere in magma genesis at active continental margins. In: *Continental Basalts and Mantle Xenoliths* (eds. C.J. Hawkesworth and M.J. Norry): 230–249. Shiva, Nantwich.
- Pearce, J.A., 1996.** A user's guide to basalt discrimination diagrams. Geological Association of Canada, Short Course Notes, **12**: 79–113.
- Pearce, J.A., 2008.** Geochemical fingerprinting of oceanic basalts with applications to ophiolite classification and the search for Archean oceanic crust. *Lithos*, **100**: 14–48.
- Pearce, J.A., Cann, J.R., 1973.** Tectonic setting of basic volcanic rocks determined using trace element analyses. *Earth and Planetary Science Letters*, **19**: 290–300.
- Pearce, J.A., Norry, M.J., 1979.** Petrogenetic implications of Ti, Zr, Y, and Nb variations in volcanic rocks. *Contributions to Mineralogy and Petrology*, **69**: 33–47.
- Petrascheck, W., 1909.** Ergebnisse neuer Aufschlüsse im Randgebiete des galizischen Karbons. *Verhandlungen der Geologischen Bundesanstalt*, **16**: 366–378.
- Plyusnina, L.P., 1982.** Geothermometry and geobarometry of plagioclase-hornblende bearing assemblages. *Contributions to Mineralogy and Petrology*, **80**: 140–146.
- Ravna, E.J.K., 2000.** Distribution of Fe and Mg between coexisting garnet and hornblende in synthetic and natural systems: an empirical calibration of the garnet-hornblende Fe-Mg geothermometer. *Lithos*, **53**: 265–277.
- Saccani, E., 2015.** A new method of discriminating different types of post-Archean ophiolitic basalts and their tectonic significance using Th-Nb and Ce-Dy-Yb systematics. *Geoscience Frontiers*, **6**: 481–501.
- Saunders, A.D., Tarney, J., 1984.** Geochemical characteristics of basaltic volcanism within back-arc basins. Geological Society Special Publications, **16**: 59–76.
- Sawyer, E.W., 2008.** Atlas of Migmatites. The Canadian Mineralogist, Special Publication 9, NRC Research Press, Ottawa, Ontario, Canada.
- Schandl, E.S., Gorton, M.P., 2002.** Applications of high field strength elements to discriminate tectonic setting in VMS environments. *Economic Geology*, **97**: 629–642.
- Schmidt, M.W., 1992.** Amphibole composition in tonalite as a function of pressure: an experimental calibration of the Al-in-hornblende barometer. *Contributions to Mineralogy and Petrology*, **110**: 304–310.
- Shand, S.J., 1943.** Eruptive Rocks. Their Genesis, Composition, Classification, and Their Relation to Ore-Deposits with a Chapter on Meteorite. John Wiley & Son, New York.
- Shervais, J.W., 1982.** Ti-V plots and the petrogenesis of modern and ophiolitic lavas. *Earth and Planetary Science Letters*, **59**: 10–118.
- Spandler, C., Hermann, J., Arculus, R.J., Mavrogenes, J., 2004.** Geochemical heterogeneity and element mobility in deeply subducted oceanic crust; insights from high pressure mafic rocks from New Caledonia. *Chemical Geology*, **206**: 21–42.
- Stern, R.J., 2002.** Crustal evolution in the East African Orogen: a neodymium isotopic perspective. *Journal of African Earth Sciences*, **34**: 109–117.
- Sun, S.-S., McDonough, W.F., 1989.** Chemical and isotopic systematics of oceanic basalts: implications for mantle composition and processes. Geological Society Special Publications, **42**: 313–345.
- Taylor, S.R., McLennan, S.M., 1985.** The Continental Crust: its Composition and Evolution. Blackwell, Oxford.
- Wilson, M., 1989.** Igneous Petrogenesis. Unwin Hyman, London.
- Whitney, D.L., Evans, B.W., 2010.** Abbreviations for names of rock-forming minerals. *American Mineralogist*, **95**: 185–87.
- Winchester, J.A., Floyd, P.A., 1977.** Geochemical discrimination of different magma series and their differentiation products using immobile elements. *Chemical Geology*, **20**: 325–343.
- Wolf, M.B., Wyllie, P.J., 1994.** Dehydration-melting of amphibolite at 10 kbar: the effects of temperature and time. *Contributions to Mineralogy and Petrology*, **115**: 369–383.
- Wood, D.A., 1980.** The application of a Th-Hf-Ta diagram to problems of tectonomagmatic classification and to establishing the nature of crustal contamination of basaltic lavas of the British Tertiary volcanic province. *Earth and Planetary Science Letters*, **50**: 11–30.
- Vernon, R.H., 2011.** Microstructures of melt-bearing regional metamorphic rocks. *GSA Memoir*, **207**: 1–11.
- Yang, Z.F., Zhou, J.H., 2013.** Can we identify source lithology of basalt? *Scientific Reports*, **3**: 1856; doi: 10.1038/srep01856.
- Zhao, G.C., Cawood, P.A., Wilde, S.A., Sun, M., 2002.** Review of global 2.1–1.8 Ga orogens: implications for a pre-Rodinia supercontinent. *Earth-Science Reviews*, **59**: 125–162.
- Zhao, G.C., Li, S.Z., Sun, M., Wilde, S.A., 2011.** Assembly, accretion, and break-up of the Palaeo-Mesoproterozoic Columbia supercontinent: records in the North China Craton revisited. *International Geology Review*, **53**: 1331–1356.
- Żelaźniewicz, A., Fanning, C.M., 2020.** Neoproterozoic fragments in the Brunovistulia terrane, S Poland: a component of the Columbia Supercontinent? *Geological Quarterly*, **64** (1): 120–129.
- Żelaźniewicz, A., Nowak, I., Bachliński, R., Larionov, A.N., Sergeev, S.A., 2005.** Cadomian versus younger deformations in the basement of the Moravo-Silesian Variscides, East Sudetes, SW Poland: U-Pb SHRIMP and Rb-Sr age data. *Geologia Sudetica*, **37**: 35–52.
- Żelaźniewicz, A., Buła, Z., Fanning, C.M., Seghedi, A., Żaba, J., 2009.** More evidence on Neoproterozoic terranes in southern Poland and southeastern Romania. *Geological Quarterly*, **53** (1): 93–124.
- Żelaźniewicz, A., Oberc-Dziedzic, T., Slama, J., 2020.** Baltica and the Cadomian orogen in the Ediacaran-Cambrian: a perspective from SE Poland. *International Journal of Earth Sciences*, **109**: 1503–1528.